

## Original Article

**Cite this article:** Shakerardakani F, Neubauer F, Liu X, Dong Y, Monfaredi B, and Li X-H (2021) New detrital zircon U–Pb insights on the palaeogeographic origin of the central Sanandaj–Sirjan zone, Iran. *Geological Magazine* 158: 2165–2186. <https://doi.org/10.1017/S0016756821000728>

Received: 10 February 2021

Revised: 20 June 2021

Accepted: 22 June 2021

First published online: 26 August 2021

**Keywords:**

Iranian microcontinent; Sanandaj–Sirjan metamorphic zone; U–Pb geochronology; detrital zircon; North Gondwana; palaeobiogeography

**Author for correspondence:**

Farzaneh Shakerardakani,  
Email: [farzaneh.shakerardakani@sbg.ac.at](mailto:farzaneh.shakerardakani@sbg.ac.at)

# New detrital zircon U–Pb insights on the palaeogeographic origin of the central Sanandaj–Sirjan zone, Iran

Farzaneh Shakerardakani<sup>1,2,3</sup> , Franz Neubauer<sup>1</sup>, Xiaoming Liu<sup>4</sup>, Yunpeng Dong<sup>4</sup>, Behzad Monfaredi<sup>5</sup> and Xian-Hua Li<sup>2,3,6</sup> 

<sup>1</sup>Department of Geography and Geology, Paris-Lodron-University of Salzburg, Hellbrunner Str. 34, A-5020 Salzburg, Austria; <sup>2</sup>State Key Laboratory of Lithospheric Evolution, Institute of Geology and Geophysics, Chinese Academy of Sciences, Beijing 100029, China; <sup>3</sup>Innovation Academy for Earth Science, Chinese Academy of Sciences, Beijing 100029, China; <sup>4</sup>State Key Laboratory of Continental Dynamics, Department of Geology, Northwest University, Northern Taibai Str. 229, Xi'an 710069, China; <sup>5</sup>Institute of Earth Sciences – NAWI Graz Geocenter, University of Graz, Universitätsplatz 2, Graz 8010, Austria and <sup>6</sup>College of Earth and Planetary Sciences, University of Chinese Academy of Sciences, Beijing 100049, China

**Abstract**

New detrital U–Pb zircon ages from the Sanandaj–Sirjan metamorphic zone in the Zagros orogenic belt allow discussion of models of the late Neoproterozoic to early Palaeozoic plate tectonic evolution and position of the Iranian microcontinent within a global framework. A total of 194 valid age values from 362 zircon grains were obtained from three garnet–micaschist samples. The most abundant detrital zircon population included Ediacaran ages, with the main age peak at 0.60 Ga. Other significant age peaks are at *c.* 0.64–0.78 Ga, 0.80–0.91 Ga, 0.94–1.1 Ga, 1.8–2.0 Ga and 2.1–2.5 Ga. The various Palaeozoic zircon age peaks could be explained by sediment supply from sources within the Iranian microcontinent. However, Precambrian ages were found, implying a non-Iranian provenance or recycling of upper Ediacaran–Palaeozoic clastic rocks. Trace-element geochemical fingerprints show that most detrital zircons were sourced from continental magmatic settings. In this study, the late Grenvillian age population at *c.* 0.94–1.1 Ga is used to unravel the palaeogeographic origin of the Sanandaj–Sirjan metamorphic zone. This Grenvillian detrital age population relates to the ‘Gondwana superfan’ sediments, as found in many Gondwana-derived terranes within the European Variscides and Turkish terranes, but also to units further east, e.g. in the South China block. Biogeographic evidence proves that the Iranian microcontinent developed on the same North Gondwana margin extending from the South China block via Iran further to the west.

**1. Introduction**

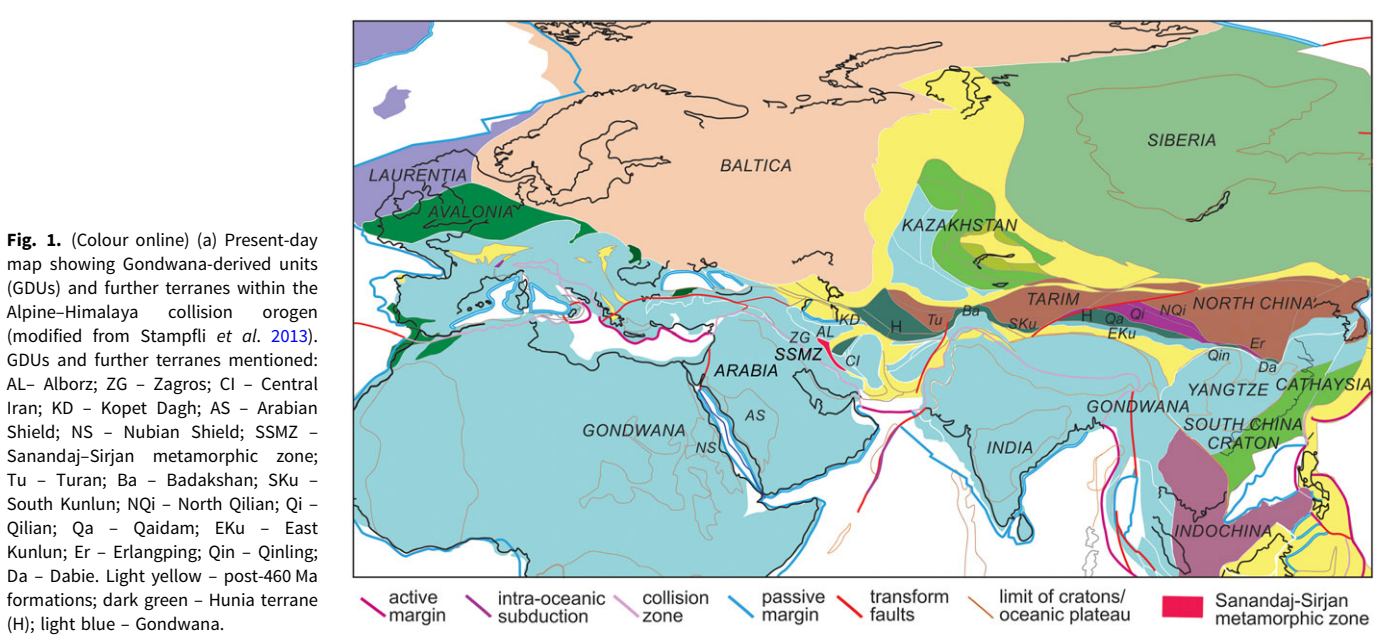
The Gondwana supercontinent is the result of large-scale amalgamation of continents and microcontinents located within East and West Gondwana. Amalgamation started at the end of the Neoproterozoic period, which led to the formation of the East African orogen (e.g. Stern, 1994; Collins & Pisarevsky, 2005; Stampfli *et al.* 2013; Meinhold *et al.* 2013) and consequently records the first stage in the development of the Transgondwanan Supermountain (Squire *et al.* 2006). From the northern margin of Gondwana, major terranes split off during Palaeozoic time (Şengör, 1990 and references therein), moved to the north and were accreted to the Eurasian margin during Triassic and Cenozoic times (e.g. Agard *et al.* 2011; Abbo *et al.* 2015; Hassanzadeh & Wernicke, 2016; Stephan *et al.* 2019). Understanding the exact origin of these Gondwana-derived terranes along the Gondwana margin has been a major geological challenge in the last decade (e.g. Stampfli *et al.* 2013; von Raumer *et al.* 2013; Stephan *et al.* 2019; Žák *et al.* 2021; Fig. 1).

Although most of the Neoproterozoic palaeogeographic reconstructions place the Iranian microcontinent along the Prototethyan margin of northern Gondwana, which is close to the East African orogen (e.g. Hassanzadeh *et al.* 2008; Horton *et al.* 2008; Fergusson *et al.* 2016), some new age information and the tectonic setting of the Neoproterozoic rocks indicate that the Iranian microcontinent was originally part of a series of peri-Gondwanan terranes, similar to the Avalonian (640–540 Ma) and Cadomian (616–540 Ma) arc terranes (e.g. Murphy *et al.* 2004; Moghadam *et al.* 2020b; Fig. 1).

The age and nature of the continental crust in Iran have been documented during previous research, including zircon U–Pb ages published over the last two decades that demonstrate the dominance of Pan-African continental crustal material in the Iranian microcontinent, recording widespread late Neoproterozoic subduction-related magmatism (e.g. Ramezani & Tucker, 2003; Hassanzadeh *et al.* 2008; Rahmati-Illkchi *et al.* 2011; Jamshidi Badr *et al.* 2013; Nutman *et al.*

© The Author(s), 2021. Published by Cambridge University Press. This is an Open Access article, distributed under the terms of the Creative Commons Attribution licence (<http://creativecommons.org/licenses/by/4.0/>), which permits unrestricted re-use, distribution and reproduction, provided the original article is properly cited.

**CAMBRIDGE**  
UNIVERSITY PRESS



2014; Shakerardakani *et al.* 2015; Fergusson *et al.* 2016; Moghadam *et al.* 2018, 2020b). Recent research on amphibolites in the central Sanandaj–Sirjan metamorphic zone (SSMZ) identified Neoproterozoic xenocrystic zircons that revealed the presence of hidden Neoproterozoic crustal components in Iran (Shakerardakani *et al.* 2019).

In addition, detrital zircon data from Neoproterozoic, Palaeozoic and Triassic clastic sediments have recently become available from many different portions of the Iranian microcontinent, such as from the central Alborz, Zagros, northwestern Central Iranian terrane and NE Iran (e.g. Horton *et al.* 2008; Etemad-Saeed *et al.* 2015; Honarmand *et al.* 2016; Zhang *et al.* 2017; Moghadam *et al.* 2017; Meinhold *et al.* 2020; Zoleikhaei *et al.* 2020).

Previous detrital zircon studies indicated that the dominant age population in the upper Neoproterozoic–Cambrian sandstones from the Kahar, Bayandor, Barut, Lalun and Mila formations of the Alborz and Zagros mountains is Neoproterozoic, with a main age peak at 0.6 Ga as well as minor peaks at 1.0 Ga, 1.8 Ga and 2.5 Ga (Horton *et al.* 2008). In the central Alborz Mountains, alongside the youngest, prominent (0.55–0.56 Ga) detrital zircon population, 0.9–1.0 Ga, 2.0–2.2 Ga, 2.5–2.7 Ga and 2.9–3.2 Ga age populations appear in the Neoproterozoic sandstones from the Kahar Formation (Etemad-Saeed *et al.* 2015). In addition, Cambrian sandstones of the Lalun Formation reveal similar reoccurring age clusters as observed in the Kahar Formation, dominated by Cryogenian–Ediacaran ages, with pre-Neoproterozoic and Cambrian zircon grains a minor component (Zoleikhaei *et al.* 2020). Some Neoproterozoic sandstones from the Kahar and Bayandor formations in Central Iran are dominated by 0.62–0.64 Ga zircon ages, with minor age populations at 0.82 Ga, 0.92–0.94 Ga, 1.9–2.3 Ga and 2.5–3.0 Ga (Honarmand *et al.* 2016). The dominant age population from Cambrian sandstones of the Zaigun Formation is Cryogenian to Tonian (Grenvillian) (0.7–0.9 Ga), with subordinate Palaeoproterozoic to Neoproterozoic (2.4–2.6 Ga) populations. However, the Triassic Nakhllak Group sandstones of Central Iran show a pronounced age population at c. 240–280 Ma, with subordinate pre-Permian Palaeozoic peaks at c. 320 Ma and 480 Ma. Meinhold *et al.*

(2020) suggested sediment supply from the Permian–Triassic magmatic rocks of the Silk Road Arc further north. The Neoproterozoic and Palaeoproterozoic zircons have predominantly rounded shapes suggesting recycling of older sedimentary rocks (Meinhold *et al.* 2020). In NE Iran, the Ordovician to Lower Devonian sandstones are characterized by distinct age groups at 2.5 Ga, 0.6–0.8 Ga, 0.5 Ga and 0.4–0.5 Ga, as well as a minor age peak at 1.0 Ga (Moghadam *et al.* 2017).

In this paper, we carry out, for the first time, a coupled U–Pb age and trace-element analysis of detrital zircons from three garnet-micaschist samples (primarily Neoproterozoic–early Palaeozoic in age) distributed along a ~100 km long central segment of the SSMZ in the Zagros orogenic belt (Fig. 1). For the interpretation of our results, we integrate our new data with the previously published detrital zircon U–Pb data from other Precambrian–Palaeozoic clastic sediments throughout the Alborz, Central Iran and NE Iran. We juxtapose the new detrital U–Pb zircon data with biogeographic evidence to constrain the position of the Iranian microcontinent on the northern Gondwana margin and its relation to the global framework as was recently also postulated by Yang *et al.* (2020) and Merdith *et al.* (2021). We show that the SSMZ as part of the Iranian microcontinent bears similar detrital zircon age spectra to those known from the Arabian–Nubian shield, in peri-Gondwanan terranes to the west of Iran as well as to those of the South China block in the east.

## 2. Geological background

Iran is regarded as a fragment of Gondwana and comprises several blocks or domains, e.g. the Alborz and Zagros mountain belts, the Central Iranian plateau and the Kopet Dagh Mountains, that are separated by deep-seated faults or suture zones (e.g. Stöcklin, 1968; Berberian & King, 1981; Fig. 1). Major areas of exposed crystalline basement rocks with variable dimensions occur within all of the continental tectonic zones in Iran barring the Kopet Dagh Mountains to the northeast.

The NW–SE-trending Zagros orogen of western Iran is part of the Alpine–Himalayan orogenic belt and developed as the result of the continental collision between the African–Arabian continent

and the Iranian microcontinent (e.g. Berberian & King, 1981; Alavi, 1994; Mohajjel *et al.* 2003; Agard *et al.* 2011; Mouthereau *et al.* 2012). The Zagros Mountains are subdivided into four parallel tectonostratigraphic zones, namely (from NE to SW) the Urumieh–Dokhtar magmatic arc (UDMA), the SSMZ, the Imbricate zone or High Zagros, and the Zagros fold–thrust belt (Stöcklin, 1968; Falcon, 1974; Alavi, 1994; Fig. 2a).

The SSMZ forms the innermost crystalline part of the Zagros orogen, where the continental and oceanic units were tectonically juxtaposed against the Arabian plate along the Main Zagros thrust (e.g. Agard *et al.* 2011; Hassanzadeh & Wernicke, 2016). The SSMZ is primarily composed of Precambrian–Palaeozoic metamorphic and sedimentary sequences, which are unconformably overlain by Permian–Triassic marbles, Jurassic phyllites and Aptian–Albian limestones (Stöcklin, 1968; Berberian & King, 1981). In addition, this zone represents the largest exposure and well-preserved record of key events during late Palaeozoic to middle Cenozoic times, which represent the formation and destruction of the Neotethys Ocean (e.g. Mohajjel *et al.* 2003; Hassanzadeh & Wernicke, 2016). The SSMZ, Central Iran and (southern and central) Alborz are considered part of the Iranian microcontinent, bearing a similar late Ediacaran–Palaeozoic and Mesozoic stratigraphy (e.g. Hassanzadeh & Wernicke, 2016; Moghadam *et al.* 2017 and references therein).

### 3. Geological setting and sampling

#### 3.a. Dorud–Azna area

The Dorud–Azna region is located in the central part of the SSMZ close to the Main Zagros thrust, which is known to comprise a polyphase metamorphic succession (Mohajjel *et al.* 2003; Nutman *et al.* 2014; Shakerardakani *et al.* 2015, 2021; Fig. 2b). Structural studies and our previous U–Pb zircon dating work on this area demonstrated three metamorphic units, which are from footwall to hangingwall (Fig. 2b): (1) the Triassic June Complex, metamorphosed within greenschist-facies conditions; overlain by (2) the amphibolite-grade metamorphic Pan-African Galeh-Doz orthogneiss, which is intruded by some mafic dykes, and (3) the Amphibolite–Metagabbro unit, which includes Carboniferous metagabbro bodies (Shakerardakani *et al.* 2015; Fergusson *et al.* 2016), Carboniferous granitic orthogneiss (Shabanian *et al.* 2020) and undated amphibolites. These units have almost invariably undergone a complex history of repeated shearing, folding and transposition of ductile fabrics, which are associated with polyphase Jurassic and Cretaceous greenschist- to amphibolite-facies metamorphism. In the eastern part, the overlying low-grade metamorphic Triassic sequence is intruded by the Upper Jurassic Darijune gabbro (Shakerardakani *et al.* 2015).

The metapelitic rocks studied in this work occur in several small outcrops within the Amphibolite–Metagabbro unit in contact with metagabbro over more than 1 km around Dare-Hedavand village (Fig. 2b). The studied micaschist is brown, exhibits a weak schistosity and consists of garnet, plagioclase, quartz, K-feldspar, biotite and chlorite (Fig. 3a, b).

#### 3.b. Muteh–Golpaygan metamorphic complex

The Muteh–Golpaygan metamorphic complex is located close to the northeastern boundary of the central SSMZ, close to the UDMA within the hinterland of the Zagros orogen (Fig. 2c). The Muteh–Golpaygan metamorphic complex is generally bounded by NE–SW- to E–W-trending high-angle normal faults

that dip outward from the centre of the complex and juxtapose it against unmetamorphosed rocks in the hangingwall (Moosavi *et al.* 2014; Shakerardakani *et al.* 2019, 2020). Besides rare remnants of Neoproterozoic rocks, the Muteh–Golpaygan metamorphic complex comprises mainly Neoproterozoic basement material dominated by granitic orthogneisses and metapelites locally inter-layered with marbles along with minor quartzite (e.g. Thiele, 1966; Rachidnejad-Omran *et al.* 2002; Moritz *et al.* 2006; Moosavi *et al.* 2014; Hassanzadeh & Wernicke, 2016). All these lithologies are cross-cut by abundant leucogranitic rocks and dykes in the western part of the complex (Shakerardakani *et al.* 2020). The Neoproterozoic basement of the Muteh–Golpaygan metamorphic complex has recently been constrained by  $^{207}\text{Pb}$ – $^{206}\text{Pb}$  ages of *c.* 2.7 and 2.5 Ga from xenocrystic zircons within amphibolite (Shakerardakani *et al.* 2019). Unmetamorphic to very low-grade metamorphic Mesozoic and Cenozoic shale, sandstone, siltstone, slate, dolomite and conglomerate units overlie the basement rocks in the study area and are in turn mostly covered by Quaternary rocks.

The depositional age of the metapelitic rocks from the Muteh–Golpaygan metamorphic complex is unknown. The metapelites are dominantly characterized by amphibolite-facies mineral assemblages, including garnet, staurolite and kyanite (Moritz *et al.* 2006). K–Ar amphibole ages of *c.* 156 Ma (Rachidnejad-Omran *et al.* 2002) suggest that metamorphism was predominantly of Late Jurassic age (Moosavi *et al.* 2014; Hassanzadeh & Wernicke, 2016). Samples GQ-12 and GQ-21 are strongly foliated garnet-micaschists from the Muteh–Golpaygan metamorphic complex (Fig. 3c, d) and consist of biotite, porphyroblastic garnet (up to 1 mm in size), white mica, plagioclase, chlorite and opaque phases.

### 4. Analytical methods

In this study, we analysed the detrital zircon populations of three garnet-micaschist samples from the SSMZ to gain insight into the provenance of these strata and how it changes through time and along the SSMZ. Two samples, GQ-12 and GQ-21, were collected to the north of the Muteh–Golpaygan metamorphic complex, while the third sample, LJ-140, was collected northeast of the Dorud area (Fig. 2b; online Supplementary Material Table S1). All three samples contain abundant zircon grains.

Zircons were extracted from a garnet-micaschist (sample LJ-140) of the Dorud–Azna region at Salzburg University. About 3 kg of each sample was crushed in a steel disc mill to obtain the ~50–250  $\mu\text{m}$  sieve fraction. Zircons were concentrated by a standard plastic pan and warm water, Frantz isodynamic magnetic separator and methylene iodide heavy liquid separation procedures, and handpicking under a binocular microscope. A total of 130 zircon grains were dated *in situ* on an excimer (193 nm wavelength) laser ablation inductively coupled plasma mass spectrometer (LA-ICP-MS) at the State Key Laboratory of Continental Dynamics, Northwest University, Xi'an, China. Trace elements were measured simultaneously. The analytical details follow Liu *et al.* (2008) and are described in Appendix 1.

U–Pb and trace-element analysis of a total of 228 detrital zircon grains obtained from two garnet-micaschist samples (GQ-12 and GQ-21) within the Muteh–Golpaygan metamorphic complex was performed at the China University of Geosciences, Beijing by LA-ICP-MS, using the methodology of Song *et al.* (2010). Detrital zircon grains (~50–200  $\mu\text{m}$ ) were separated from crushed rocks using a standard plastic pan and warm water and subsequent magnetic

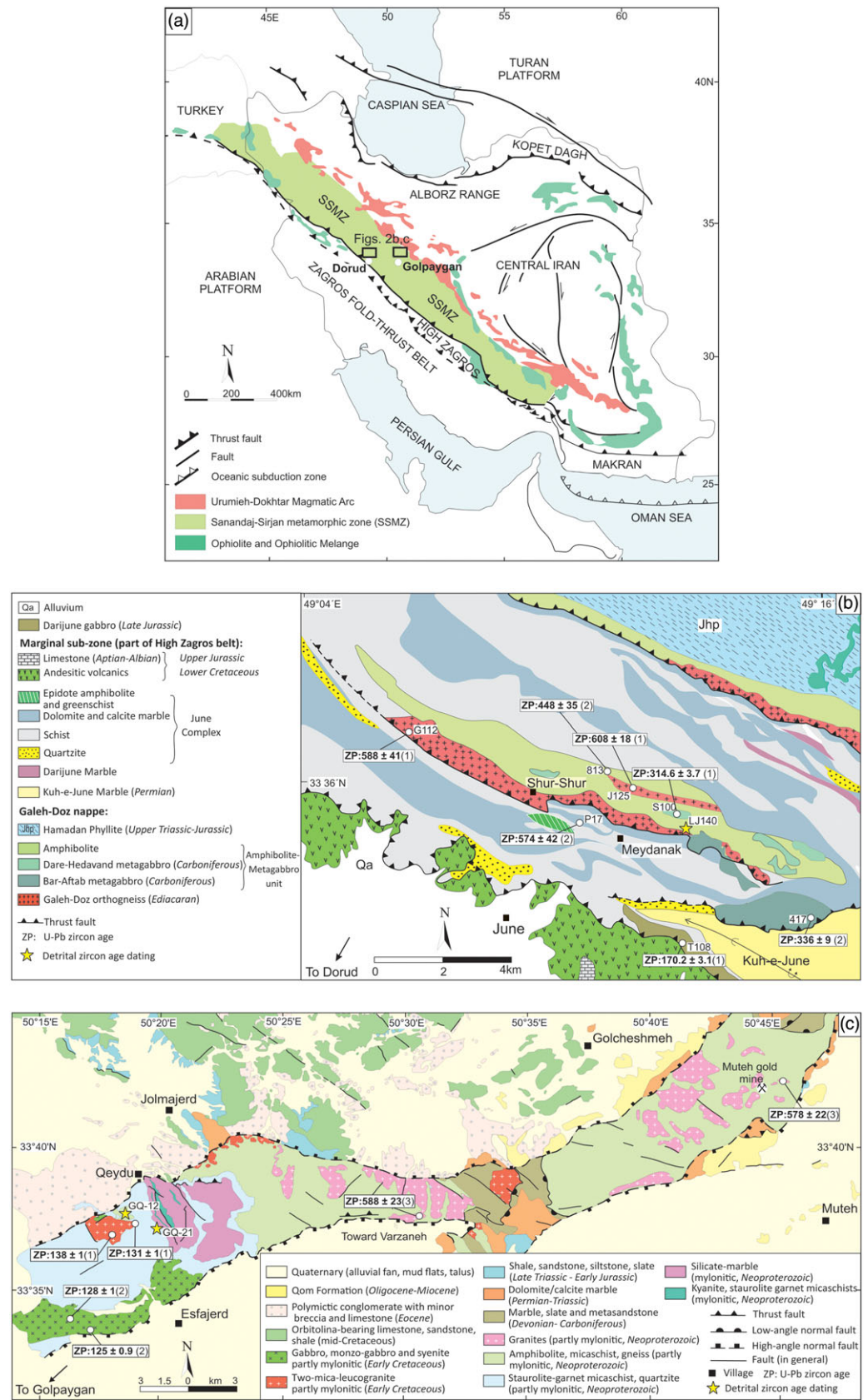


**Fig. 2.** (Colour online) (a) Main zones under consideration in Iran. (b) Simplified geological map of the Dorud-Azna region and sample location of garnet-micaschist. Ages are given in Ma; sources of data: 1 – Shakerardakani *et al.* (2015); 2 – Fergusson *et al.* (2016). (c) Geological map of the Muteh-Golpaygan area and location of investigated samples (modified after Shakerardakani *et al.* 2020 and references therein). Sources of data: 1 – Shakerardakani *et al.* (2020); 2 – unpublished data; 3 – Hassanzadeh *et al.* (2008).

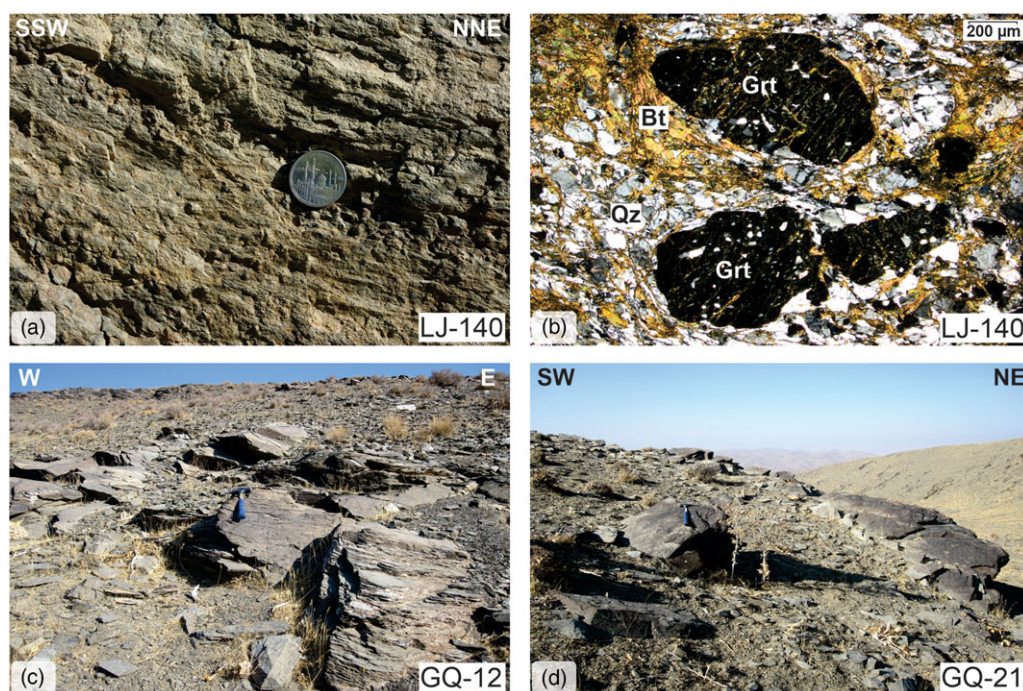


**Fig. 3.** (Colour online) (a, c, d) Field photographs of schist outcrop sampled in the study and (b) representative photomicrograph of schist. (a) Foliated garnet-micaschist in the Dorud-Azna area. Diameter of coin for scale is 29.3 mm. (b) Large garnet porphyroclasts in the matrix composed of quartz, plagioclase, K-feldspar and biotite. (c, d) Strongly foliated garnet-micaschists of the Muteh-Golpaygan area. Length of hammer for scale is 33 cm.

separation and heavy liquid separation followed by handpicking. The analytical details are given in Appendix 2.

For interpretation of the age data, we used the recent version (<http://www.stratigraphy.org>) of the time-scale calibration proposed by Cohen *et al.* (2013).

## 5. Analytical results

Together, we carried out a coupled U–Pb age and trace-element analysis of 362 detrital zircons from three garnet-micaschist samples (primarily Palaeozoic–early Mesozoic in age, see Sections 5.a and 5.b) distributed along a ~100 km long section of the central SSMZ, and they can be taken as representative of the central part of the SSMZ.

### 5.a. Detrital zircon ages: Dorud–Azna area

Zircons from sample LJ-140 have crystal lengths of ~70 to 200  $\mu\text{m}$ . Except those with an early Proterozoic age or with an age at the middle/late Proterozoic boundary, most grains are euhedral or subeuhedral, implying relatively short transport. As shown in representative cathodoluminescence (CL) images (Fig. 4), the majority of the investigated zircon grains exhibit clear inner structures with a broad zoning, an internal oscillatory zoning and very rarely thin bright rims under CL, interpreted as metamorphic overgrowths. Zircons have Th and U contents ranging from 2.06 to 1357 ppm and 34.21 to 2618 ppm, respectively. The Th/U ratios range from 0.10 to 1.78 with a mean value of 0.53, except four spots (Th/U < 0.1), indicating that the majority of the zircons are of magmatic origin (Corfu *et al.* 2003; Corfu, 2004).

In total, 134 analyses were obtained for 130 zircon grains from the garnet-micaschist sample; 30 analyses are not considered because of a discordance of > 10 %, and 104 grains are subconcordant between 90 and 110 % concordancy (Fig. 5; online

Supplementary Material Table S1). The majority of the zircon populations (96 %) contain grouping of 565–700 Ma, 737–805 Ma, 820–915 Ma, 0.93–1.1 Ga, 1.81–2.07 Ga, 2.14–2.5 Ga and one younger, Cambrian age (~507 Ma). Owing to low Th/U ratios and missing oscillatory zoning, four zircons ( $507 \pm 9$  Ma,  $586 \pm 8$  Ma,  $692 \pm 9$  Ma and  $702 \pm 11$  Ma) are interpreted as metamorphic zircons. Only four Archaean ages (< 4 %) were discovered (~2.62, 2.68, 2.73 and 3.24 Ga).

### 5.b. Detrital zircon ages: Muteh–Golpaygan metamorphic complex

A total of 90 valid age values out of 228 zircon grains were obtained based on whether their U–Pb analyses were concordant or not.

Most zircon grains from the sample GQ-21 are euhedral to subeuhedral prisms (50 to 150  $\mu\text{m}$  in length) with a clear oscillatory (e.g. spot 50) and/or sector zoning (e.g. spots 41, 87) in CL images and Th/U ratios ranging from 0.11 to 3.13, suggesting that they have a magmatic origin (Figs 4, 6). However, nine zircon grains appear homogeneous in CL images and were recorded to possess low Th/U ratios of 0.03 to 0.07; these characteristics typically imply a metamorphic origin (e.g. Rubatto, 2002).

Zircon U–Pb analyses yielded diverse age groups, indicating different sources for the zircons (Fig. 5). Six major age populations dominate the GQ-21 detrital zircon grains, with populations at 547–611 Ma, 642–788 Ma, 868–931 Ma, 0.97–1.17 Ga, 1.79–2.07 Ga and 2.36–2.5 Ga. From a total of 40 dated subconcordant zircons, one gave an Ordovician age (~467 Ma), two gave Cambrian ages (~505 Ma, 532 Ma) and one gave a Neoproterozoic age (~2.58 Ga; online Supplementary Material Table S1). Six Proterozoic zircons ( $1787 \pm 35$  Ma,  $1030 \pm 52$  Ma,  $642 \pm 4$  Ma,  $611 \pm 5$  Ma,  $602 \pm 5$  Ma,  $552 \pm 4$  Ma) are considered to have a metamorphic origin.

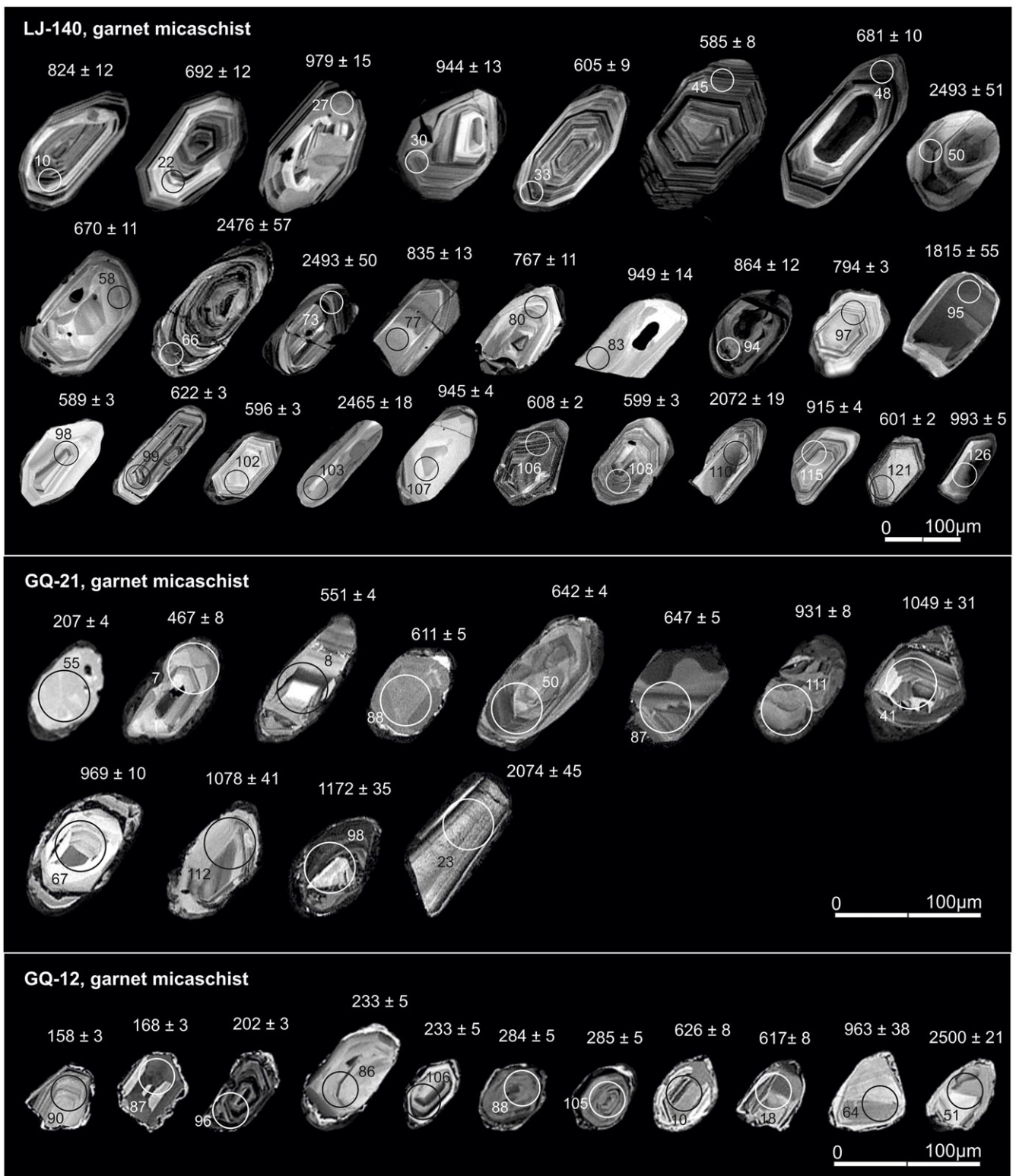


**Fig. 4.** Cathodoluminescence images of dated zircons from garnet-micaschists of the Dorud-Azna and Muteh-Golpaygan regions.  $^{206}\text{Pb}$ - $^{238}\text{U}$  age (Ma) is shown for ages <1000 Ma, the  $^{207}\text{Pb}$ - $^{206}\text{Pb}$  age when older than 1000 Ma. Circles represent analysis spot positions with spot numbers and their ages in Ma.

With the exception of few sub-rounded zircon grains in sample GQ-12, the vast majority of the zircons are nearly euhedral or sub-hedral and prismatic (~50 to 100 µm in length). Many zircons show a clear oscillatory or sector zoning in CL images, and some of them exhibit thin overgrowth rims of weak or no zoning (Fig. 4).

The Th/U ratios of the zircons range from 0.10 to 2.03, except four spots (<0.1). The U and Th concentrations range from 75.5 to 2759 ppm and from 18.21 to 2218 ppm, respectively.

The zircon age populations from sample GQ-12 span characteristic intervals of time, namely 200–323 Ma, 383–423 Ma, 559–

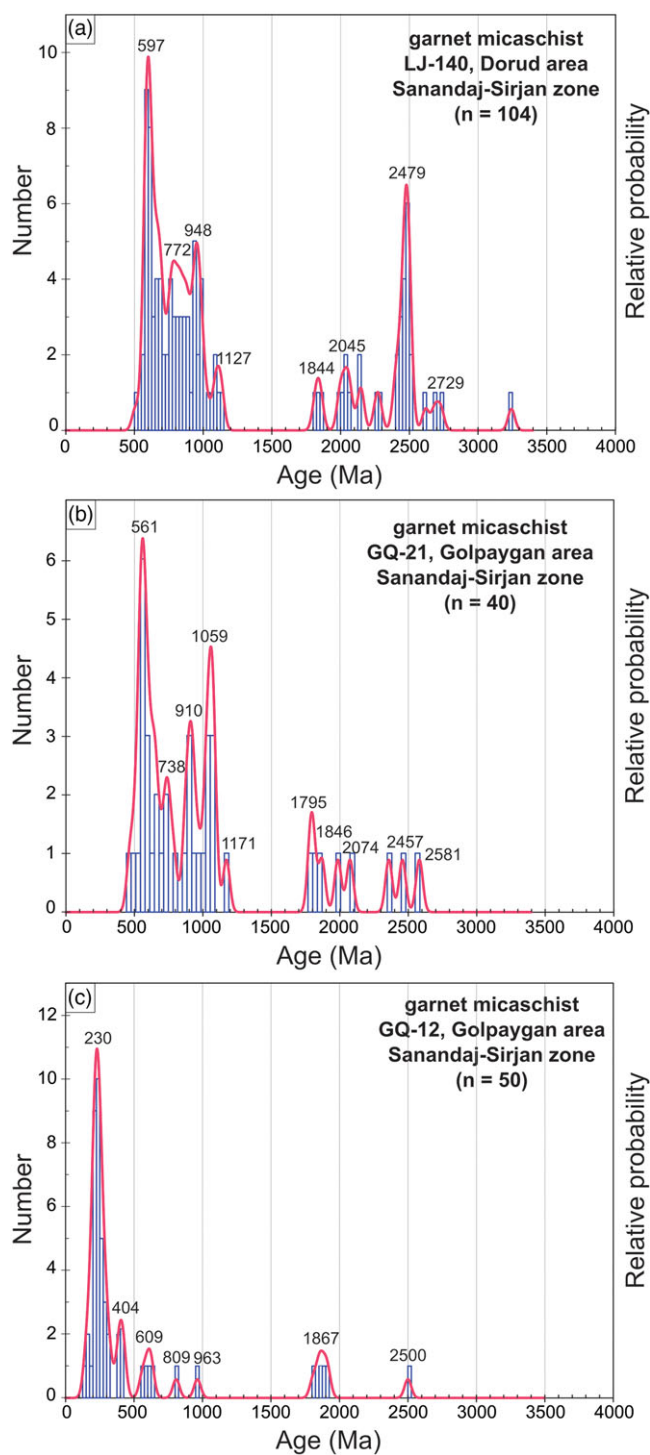


**Fig. 5.** (Colour online) Histograms and Kernel Density Estimations (KDE) for detrital zircon U–Pb ages in the studied samples. (a) Sample from the Dorud–Azna region and (b, c) Samples from the Muteh–Golpaygan region of the central Sanandaj–Sirjan metamorphic zone.

626 Ma, 808–963 Ma and 1.81–2.5 Ga, displaying a multi-peaked age distribution pattern (Fig. 5). Five out of 50 subconcordant zircons analysed have Jurassic (~149–200 Ma) ages. This sample yields a small portion (<4%) of metamorphic zircons ( $1916 \pm 24$  Ma,  $1808 \pm 21$  Ma).

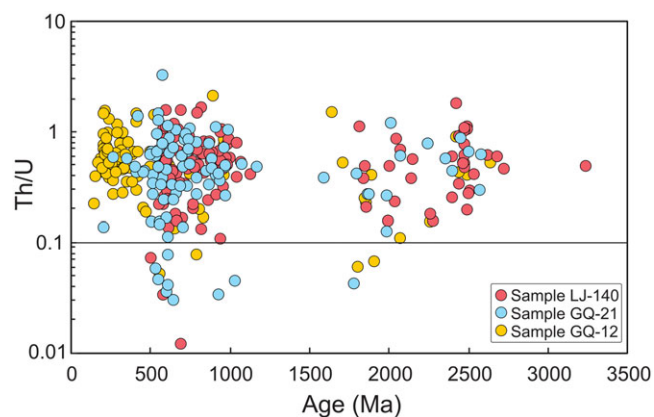


**Fig. 6.** (Colour online) Zircon Th/U ratio versus U–Pb ages of the detrital zircons from three garnet-micaschists. Note that most of the zircons from this study reside above 0.1.

### 5.c. Trace-element chemistry of the zircons

Trace-element compositions of zircon grains can identify the most likely source rock types within which the detrital zircon grains crystallized (e.g. Belousova *et al.* 2002; Hoskin & Schaltegger, 2003; Grimes *et al.* 2007, 2015; Portner *et al.* 2011; Ranjan *et al.* 2020). Chondrite-normalized rare earth element (REE) patterns (online Supplementary Material Table S2; Fig. 7) for most of the laser spots of sample LJ-140 indicate features typical for a wide variety of crustal rocks (Hoskin & Schaltegger, 2003), with heavy rare earth element (HREE) abundance between 100 $\times$  and 10 000 $\times$  chondrite. Spider plots show prominent positive and negative Ce and Eu anomalies, respectively (Fig. 7). The REE patterns, zircon internal textures and high Th/U ratios (Th/U = 0.1–1.78) suggest that a majority of the zircons are typical of magmatic protoliths with mild effects of late-magmatic/metamorphic recrystallization, as indicated by the flat HREE patterns for a few zircons (Fig. 7).

The chondrite-normalized zircon REE patterns for all age populations of sample GQ-21 show a similar pattern of depleted light rare earth elements (LREEs), progressively increasing HREEs, a prominent positive Ce anomaly and a negative Eu anomaly. These observations are consistent with the textural features indicating zircon growth from melts as a dominant process for the growth of all zircon populations (Rubatto & Hermann, 2007).

Discrimination diagrams using U/Yb or Th/Yb ratios provide a robust method for distinguishing modern zircons crystallized within continental or oceanic crust (Grimes *et al.* 2007, 2015). Generally, the U/Yb ratio is controlled by the difference in element solubility. Incompatible elements, such as U, are readily soluble in fluids and thus subsequently enriched in continental crust relative to oceanic crust and upper mantle (Grimes *et al.* 2007). Consequently, continental crust is less enriched in incompatible elements, such as Y and Yb, relative to oceanic crust (e.g. Belousova *et al.* 2002; Grimes *et al.* 2007). On the U/Yb versus Hf (and U versus Yb) diagrams, the detrital zircons in both samples plot predominantly in the field of continental zircons; based on available data they are clearly distinct from the field of oceanic crustal zircons (Fig. 8a, b). Furthermore, Grimes *et al.* (2015) have shown that the Nb/Th and Nb/U ratios of zircons reflect the ratios of their host rocks and that zircons from continental arcs have lower Nb/Th and Nb/U ratios compared to zircons in rocks from non-arc settings. Plotting the detrital zircons shows that nearly all

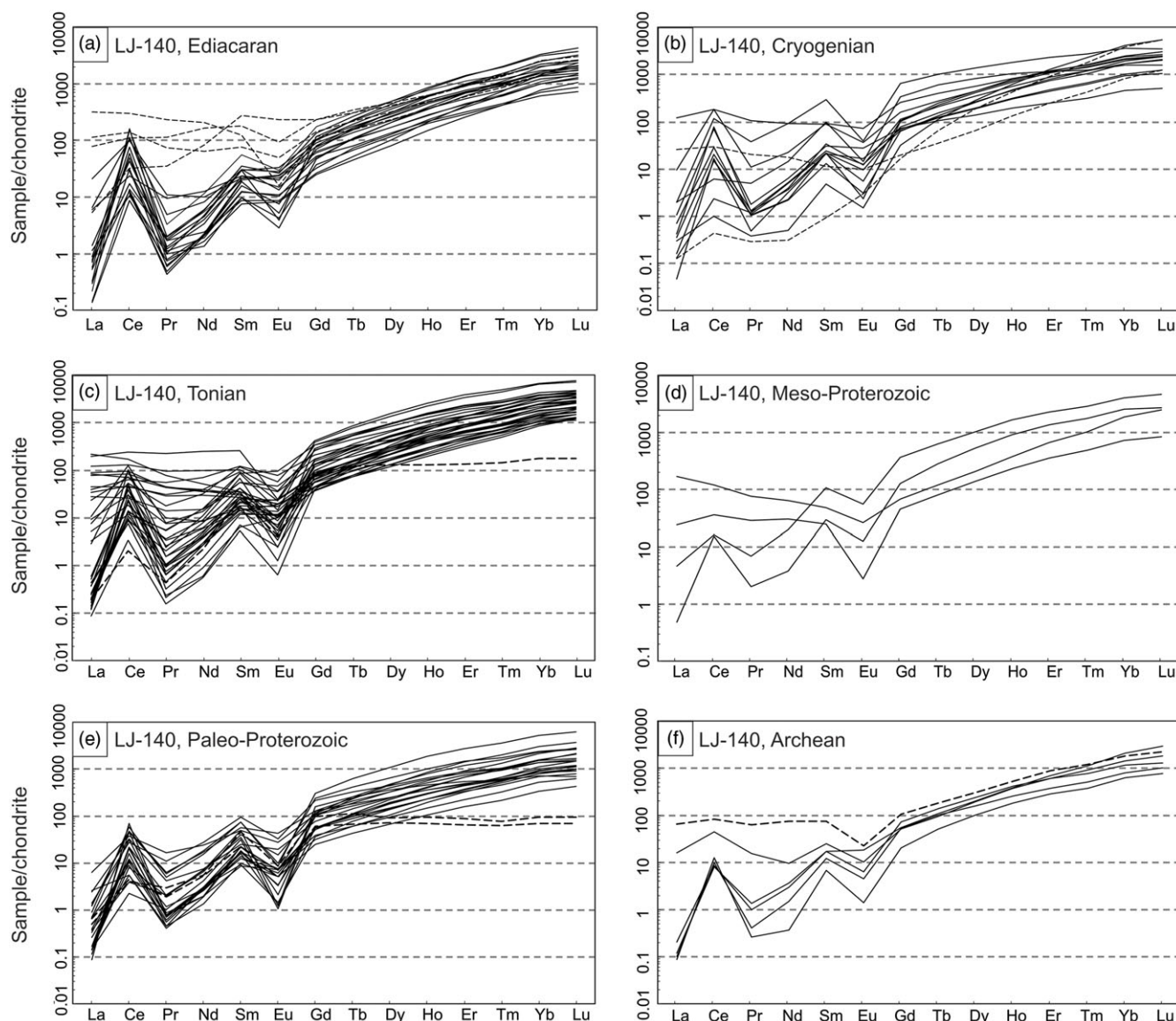


Fig. 7. Chondrite-normalized REE patterns for zircons from sample LJ-140. Chondrite data are from McDonough & Sun (1995).

of the detrital zircon populations (92–95 %) are enriched in U/Yb ratios and plot in the continental field (Fig. 8a–c). This result cannot be attributed to a homogeneous source region or derivation of detritus from a single source but was considered by Hoskin & Ireland (2000) to confirm the apparent monotony of REE patterns and abundances in zircons derived from a range of common crustal rock types (Hoskin & Schaltegger, 2003).

## 6. Discussion

### 6.a. Depositional ages

In order to determine the most reliable maximum depositional age for each sample, we utilize four alternate measures of the maximum depositional ages as outlined by Dickinson & Gehrels (2009). These include: (1) the age of the youngest single grain within a sample with a  $1\sigma$  error less than 10 Ma (e.g. Stevens Goddard *et al.* 2018); (2) the youngest graphical peak detrital zircon age controlled by more than one grain age; (3) the calculated

weighted mean age of the youngest age peak from an at least three-grain cluster with overlapping ages within the  $2\sigma$  error and a mean square weighted deviation (MSWD)  $\leq 1$ ; and (4) the weighted average age of the youngest two or more grains that overlap in age at  $1\sigma$  error.

The oldest sample in this study (sample LJ-140) was collected from the north of the Dorud–Azna region in the central SSMZ (Fig. 2b). The sample displays a prominent peak at  $577 \pm 9$  Ma, which is only  $\sim 10$  Ma younger than the Cadomian orthogneiss basement and which is in close contact with the sample ( $608 \pm 18$  Ma and  $588 \pm 41$  Ma; Shakerardakani *et al.* 2015) implying a tectonic contact between these two lithologies. This 577 Ma age provides the maximum depositional age for this unit. A grain with an age of  $507.1 \pm 9.41$  Ma possesses a low Th/U ratio of  $<0.1$  indicating metamorphic growth, which could be post-depositional.

East of the oldest sample from the central SSMZ, close to the UDMA, two samples (GQ-21 and GQ-12) were collected from the Muteh–Golpaygan metamorphic complex. The first sample

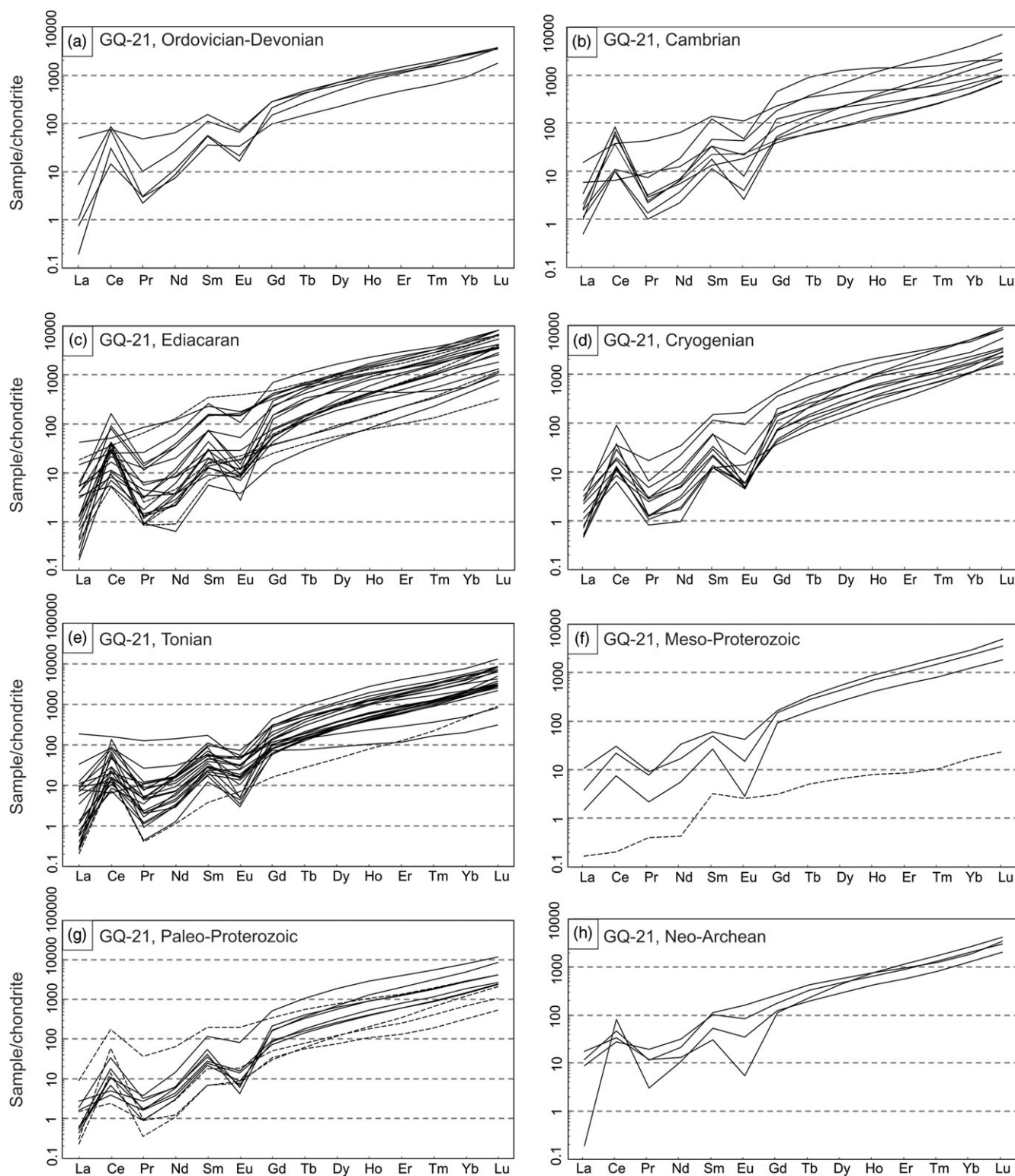
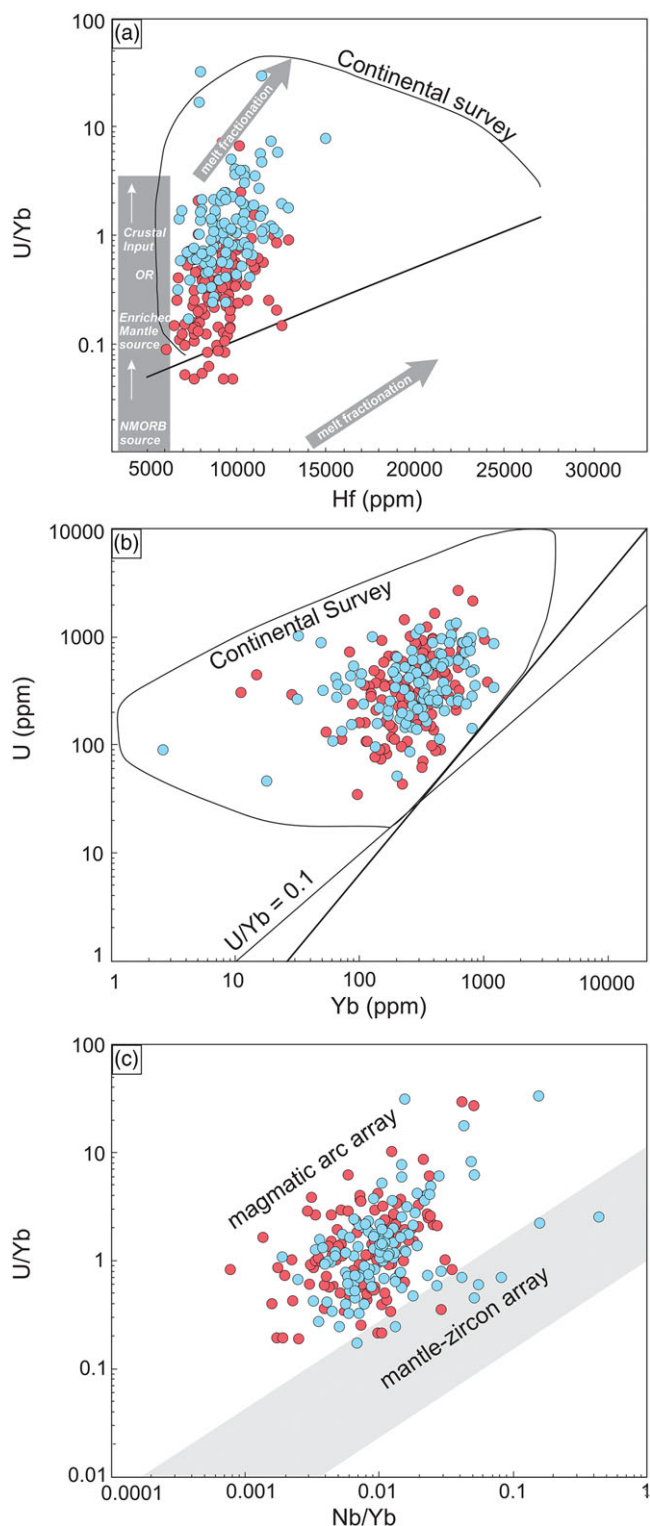


Fig. 7. (Continued) Chondrite-normalized REE patterns for zircons from sample GQ-21. Chondrite data are from McDonough & Sun (1995).

(sample GQ-21) is distinguished by its prominent peak near 561 Ma, but it also contains one Middle Ordovician ( $467 \pm 8$  Ma) and two Cambrian ( $505 \pm 4$  Ma,  $532 \pm 4$  Ma) detrital zircon grains. The weighted mean age for four grains at the prominent peak mentioned above is  $552 \pm 4$  Ma (MSDW = 0.69). The  $\sim 552$  Ma age peak for sample GQ-21 is close to the 577 Ma peak of sample

LJ-140 from the Dorud–Azna region. The youngest single grain yielding an age of  $467 \pm 8$  Ma ( $1\sigma$ ), however, may indicate a younger depositional age.

The second sample from the northwestern part of the Muteh–Golpaygan complex (GQ-12) displays a marked change in provenance to Mesozoic–Palaeozoic sources with main peaks at



**Fig. 8.** (Colour online) (a, b) U/Yb versus Hf and U versus Yb concentrations in zircon and expected generalized trends for zircon from variably incompatible element-enriched reservoirs as well as parental melt fractionation (Grimes *et al.* 2015). The field labelled 'Continental Survey' and lower bound were defined by Grimes *et al.* (2007). (c) U/Nb proxy for the tectono-magmatic source of igneous zircon. The shaded band represents a 'mantle-zircon array' defined by Grimes *et al.* (2015). The upper boundary is placed at the Nb/Yb, U/Yb endpoints (0.0004, 0.02) and (1, 10). Magmatic arc and post-collisional continental zircon are typically offset above the mantle-zircon array. NMORB – normal mid-ocean ridge basalt.

230 Ma, 404 Ma, 609 Ma and 1867 Ma (Fig. 5). The youngest peak in this sample is at the Late Triassic – Early Jurassic boundary ( $205 \pm 5$  Ma; MSDW = 1.9), and only three zircons are distinctly younger ( $149 \pm 2$  Ma,  $158 \pm 3$  Ma and  $168 \pm 3$  Ma) than the rest ( $>190$  Ma). We assume therefore a maximum depositional age of earliest Jurassic for this sample, which is reasonable as metamorphosed Jurassic sediments are widespread within the central SSMZ and represent the metamorphosed cover on the Cadomian basement (e.g. Rachidnejad-Omran *et al.* 2002; Sheikholeslami *et al.* 2003; Fazlnia *et al.* 2007; Davoudian *et al.* 2016). As geochronology constrains the age of metamorphism to the Late Jurassic period (156 Ma; Rachidnejad-Omran *et al.* 2002), the depositional age is within the short period between 205 and 156 Ma.

## 6.b. Provenance

### 6.b.1. Magmatic history of the SSMZ

Previous studies have provided a wealth of isotopic age constraints for many of the regional and long-lived magmatic events in the SSMZ (Hassanzadeh & Wernicke, 2016). Although Palaeozoic magmatic rocks are rare in Iran, compared to abundant Mesozoic and Cenozoic magmatism, they record multiphase magmatism during Ordovician–Silurian, Devonian–Carboniferous and Permian times (e.g. Berberian & King, 1981; Hassanzadeh & Wernicke, 2016; Moghadam *et al.* 2020a), suggesting major tectonic events related to the formation of the Palaeotethyan and Neotethyan oceans.

Sample GQ-12 from the northwestern Golpaygan area includes the youngest detrital zircon grains with Proterozoic, Devonian, Carboniferous, Permian and Late Triassic ages. In particular, the Late Triassic U–Pb ages of 205 to 233 Ma are prominent. Sample GQ-21 from the same area yielded grains as young as 467 Ma and lacks significant Carboniferous, Permian and Late Triassic age groups, but bears a significant Neoproterozoic age population.

The continental crust of the SSMZ was thinned during Permian and Triassic times (e.g. Zanchi *et al.* 2009a,b; Buchs *et al.* 2013; Hassanzadeh & Wernicke, 2016; Shakerardakani *et al.* 2018). This precludes the possibility that the Late Triassic zircons are of xenocrystic origin through crustal contamination during the ascent of basaltic magmas through the continental crust of the SSMZ. As suggested by Shakerardakani *et al.* (2018), this basaltic magmatism may have originated from hotspot magmas intruding into the crustal base of the thinned Sanandaj–Sirjan passive margin basement and rising up into shallow levels. The latest Triassic/earliest Jurassic maximum depositional age of sample GQ-12 corresponds in age with the Middle–Upper Triassic to Jurassic sedimentary rocks, which were deposited on the passive continental margin of the Neotethys Ocean (Hassanzadeh & Wernicke, 2016; Shakerardakani *et al.* 2018). On the other hand, an origin of Triassic zircons from Late Triassic granites of Central Iran cannot be excluded (e.g. Ramezani & Tucker, 2003). Abundant similar Early Triassic to Permian ages were recently reported by Meinhold *et al.* (2020) from Triassic sandstones of Central Iran.

Furthermore, two Carboniferous–early Permian age peaks were recorded for zircons of sample GQ-12, matching the modal age of extensive Carboniferous and earliest Permian granite-gabbro intrusive suites appearing both in the SSMZ and Central Iran, as well as in the Alborz Mountains and NE Iran (e.g. Bagheri & Stampfli, 2008; Zanchi *et al.* 2009a,b; Zanchetta *et al.* 2009, 2013; Bea *et al.* 2011; Buchs *et al.* 2013; Saccani *et al.* 2013;

Kargarbafghi *et al.* 2015; Moghadam *et al.* 2015; Shakerdakani *et al.* 2017; Honarmand *et al.* 2017; Shabani *et al.* 2020). Late Palaeozoic rifting of the future Neotethys Ocean formed ribbon continental fragments in Iran that broke away from the northern margin of Gondwana (e.g. Berberian & King, 1981; Şengör, 1990; Agard *et al.* 2011; Richards, 2015). Subsequently, after a long period of epeirogeny and significant breaks in the sedimentary record during Ordovician–Carboniferous times, the late Carboniferous to early Permian was a period of marine transgression associated with a major extensional phase that affected most parts of Iran (Berberian & King, 1981; Alavi-Naini, 2009).

The available source for the early Permian zircons (sample GQ-12) is dominated by the isolated early Permian anorogenic Hasanrobat pluton (294–288 Ma), which is located south of the Muteh–Golpaygan metamorphic complex and intruded into upper Carboniferous – lower Permian strata (Alirezai & Hassanzadeh, 2012; Honarmand *et al.* 2017). The Carboniferous ages of detrital zircons can be explained by subordinate granitic orthogneisses and metagabbros of the region (Shakerdakani *et al.* 2015; Fergusson *et al.* 2016; Shabani *et al.* 2020).

Vestiges of volcanic activity during Devonian time, mostly restricted to sill-like intrusions, dykes and lava flows interlayered within sedimentary formations, are particularly known in Alborz, Central Iran, the SSMZ, and NE and NW Iran (e.g. Assereto, 1963; Alavi & Bolourchi, 1973; Lammerer *et al.* 1984; Houshmandzadeh *et al.* 1990; Wendt *et al.* 2002, 2005; Derakhshi & Ghasemi, 2015; Ghasemi & Dayhimi, 2015). Early Devonian detrital zircons can be traced from intra-oceanic Palaeotethys subduction and continental-type magmatism (e.g. Ghazi *et al.* 2001; Zanchetta *et al.* 2013; Moghadam *et al.* 2017). The Early Devonian age population of the Golpaygan detrital zircons is scattered around 404 Ma, but it is unlikely that such zircons could be transported from NE and NW Iran across the Palaeotethys to be deposited in the future SSMZ (Moghadam *et al.* 2017). Paidar-Saravi (1989) described a range of different metavolcanic rocks, including rhyolitic, dacitic and andesitic lava, which are interlayered with schists in the Muteh–Golpaygan metamorphic complex. Rachidnejad-Omran *et al.* (2002) also mentioned the presence of metarhyolite and metavolcanic tuff. They suggested that metarhyolites together with amphibolites represent a bimodal volcanic suite and, together with the host schist and gneiss, an early Palaeozoic volcano-sedimentary complex. Our field observations show that the undated rhyolitic rocks are interlayered within a Devonian–Carboniferous unit including marble, slate and meta-sandstone and are located in close contact with schists, orthogneisses and amphibolites in the central part of the Muteh–Golpaygan metamorphic complex. Therefore, we conclude that Early Devonian detrital zircons have mostly local sources.

The same is true for the ages around 600 Ma, which are well known in Palaeozoic and Mesozoic sediments and Precambrian magmatic basement rocks in the SSMZ and Central Iran (e.g. Ramezani & Tucker, 2003; Hassanzadeh *et al.* 2008; Nutman *et al.* 2014; Shakerdakani *et al.* 2015; Moghadam *et al.* 2018, 2020b; Meinhold *et al.* 2020).

Consequently, age populations older than *c.* 600 Ma are distinctive for the derivation of the SSMZ.

### 6.b.2. Palaeogeographic relationships of the SSMZ

Detrital zircon geochronology has been widely used as a robust method with which to identify the source of sedimentary rocks (Gehrels, 2014). It also represents a powerful means of resolving the displacement history of potentially displaced terranes

(Gehrels, 2014). The palaeogeographic relationships of the SSMZ are usually considered to relate to the Arabian–Nubian shield with its Neoproterozoic magmatic arcs and back-arc complexes. Particularly interesting are the age groups of 740–760 Ma and around 826 Ma. Based on our new U–Pb zircon ages, we discuss here two potential relationships: (1) the Arabian–Nubian shield connection and (2), as an alternative, which is also supported by biogeographic relationships, the South China block connection. For comparison, age spectra of these regions are shown in Figure 9.

#### 6.b.2.a. Correlation of Gondwanan detrital zircon age spectra.

The age population clusters at 0.55–0.63 Ga, 0.64–0.78 Ga, 0.80–0.91 Ga, 0.94–1.1 Ga, 1.8–2.0 Ga and 2.1–2.5 Ga are present in nearly all samples (Fig. 5). The percentage of >540 Ma zircons in each sample generally decreases with younger stratigraphic ages, ranging from ~96 % in the oldest sample to <25 % in the youngest samples. A comparison of the Neoproterozoic and early Palaeozoic detrital zircon age spectra has important implications for the palaeotectonic reorganization at the Gondwana margin. Our data show a significant concentration of detrital zircons at 0.55–0.63 Ga, consistent with ages of widespread Pan-African subduction-related granitic basement in Iran (e.g. Ramezani & Tucker, 2003; Hassanzadeh *et al.* 2008; Nutman *et al.* 2014; Shakerdakani *et al.* 2015; Moghadam *et al.* 2018).

The age groups of *c.* 0.6–0.9 Ga compose ~35 % of all analysed zircons of samples LJ-140 and GQ-21. Based on ion-microprobe U–Pb analyses of detrital zircon grains from various Neoproterozoic to Cambrian sandstones of the Alborz and Zagros mountains and from the basement of the Central Iranian plateau, Horton *et al.* (2008) proposed that a basal clastic succession representing the earliest sedimentary record in Iran displays a provenance age signature dominated by Pan-African (0.9–0.6 Ga) rocks, which are similar to detrital zircon age spectra for age-equivalent units of the west and south in Israel, Jordan, Egypt and Saudi Arabia in northern Gondwana (e.g. Avigad *et al.* 2003, 2015, 2017; Kolodner *et al.* 2006; Meinhold *et al.* 2021). Because of the lack of significant pre-600 Ma detrital zircon ages, these authors have therefore concluded that the main sources were likely located in Pan-African basement provinces of Arabia and Africa, particularly in the Arabian–Nubian shield, although the Iranian basement may have contributed some sediment. In addition, Moghadam *et al.* (2017) suggested that the 0.6–0.5 Ga old detrital zircons belong to the local Cadomian magmatism in Iran and surroundings or, alternatively, to the Arabian–Nubian shield and other reworked continental crust of Gondwana.

Pre-Neoproterozoic zircons, grouped at *c.* 0.9–1.1 Ga (Grenvillian), *c.* 1.8–2.0 Ga (early Proterozoic A) and *c.* 2.1–2.5 Ga (early Proterozoic B) make up nearly 35 % of the total zircon ages. For the Palaeoproterozoic zircons, there is a plausible origin from the Arabian–Nubian shield and Africa with a juvenile mantle source (Honarmand *et al.* 2016; Moghadam *et al.* 2017). Variable amounts of ~980 Ma ages also occur in Palaeozoic sedimentary rocks of Saudi Arabia (Meinhold *et al.* 2021), and the Grenvillian population of our samples might have their source there. The Grenvillian detrital zircons first appear in the Alborz and Zagros succession in the upper Neoproterozoic to Cambrian formations (Horton *et al.* 2008). Zoleikhaei *et al.* (2020) recently found a minor population peak at ~980–1015 Ma in the Cambrian sandstones of the central Alborz. Nutman *et al.* (2014) reported a similar age group of 0.9–1.0 Ga with juvenile initial eHf values in inherited zircon cores of some

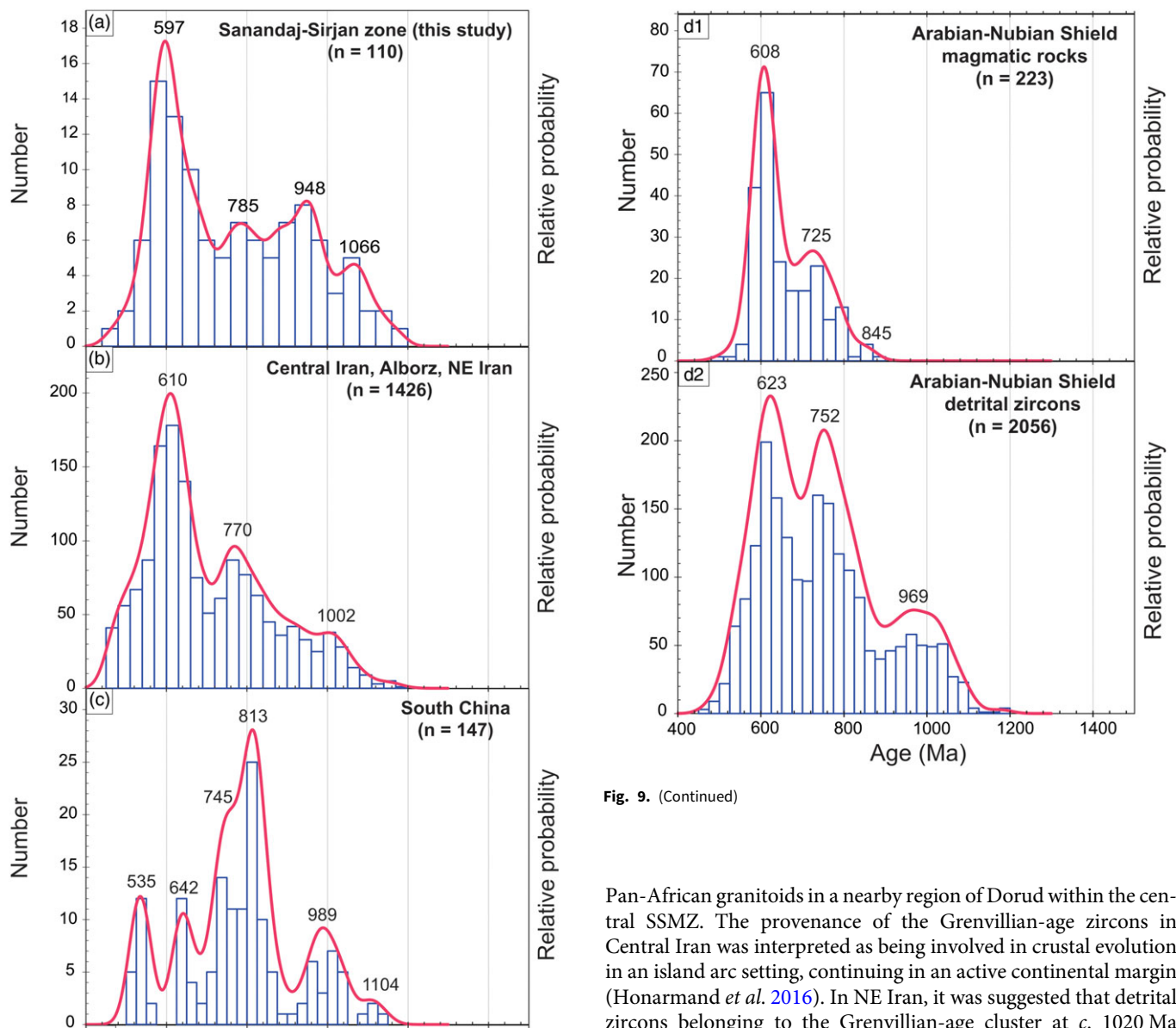


Fig. 9. (Continued)

**Fig. 9.** (Colour online) Compiled histogram and Kernel Density Estimate (KDE) of pre-460 Ma to 1400 Ma detrital zircon U-Pb ages from clastic sediments of the (a) Sanandaj-Sirjan metamorphic zone, and (b) Alborz Mts, Central Iran and NE Iran. (c) Histograms showing the magmatic age distribution in the South China block and (d1) in the Arabian-Nubian shield and its latest Neoproterozoic cover. (d2) Histogram for detrital zircon U-Pb age distribution for Neoproterozoic-Cambrian sedimentary units within the Arabian-Nubian shield. Data sources: (a, b) Shakerardakani *et al.* (2019 and references therein); Meinhold *et al.* (2020); Zoleikhaei *et al.* (2020). (c) Condon *et al.* (2005); Liu *et al.* (2008); Compston *et al.* (2008); Dong *et al.* (2012); Charvet (2013); Zhao *et al.* (2013); Wang *et al.* (2013); Li *et al.* (2014 and references therein); Yao *et al.* (2014); Du *et al.* (2014); Okada *et al.* (2014); Lan *et al.* (2015 and references therein); Yang *et al.* (2016 and references therein); Yang *et al.* (2017 and references therein); Lan *et al.* (2017); Wang *et al.* (2018, 2019, 2020). (d1) Hedge (1984); Pallister *et al.* (1988); Stern (1994); Andersen *et al.* (2009); Bea *et al.* (2009); Be'eri-Shlevin *et al.* (2009); Ali, B. H. *et al.* (2009); Ali, K. A. *et al.* (2009, 2010, 2014, 2015); Kennedy *et al.* (2010, 2011a,b); Morag *et al.* (2011); Johnson *et al.* (2011 and references therein); Augland *et al.* (2012); Johnson *et al.* (2013); Robinson *et al.* (2014); Yeshanew *et al.* (2015); Hassan *et al.* (2016); Kozdrój *et al.* (2018 and references therein); Cox *et al.* (2019); Ghanem *et al.* (2020); Abbo *et al.* (2020); Khudeir *et al.* (2021). (d2) Avigad *et al.* (2003); Morag *et al.* (2012); Li *et al.* (2018); Abd El-Rahman *et al.* (2019); Meinhold *et al.* (2021).

Pan-African granitoids in a nearby region of Dorud within the central SSMZ. The provenance of the Grenvillian-age zircons in Central Iran was interpreted as being involved in crustal evolution in an island arc setting, continuing in an active continental margin (Honarmand *et al.* 2016). In NE Iran, it was suggested that detrital zircons belonging to the Grenvillian-age cluster at *c.* 1020 Ma might be derived from a basement like that found in a sliver of Sinai basement rocks or lower Palaeozoic sandstones from Libya and Jordan (Be'eri-Shlevin *et al.* 2012; Moghadam *et al.* 2017).

The distribution of *c.* 1.0 Ga detritus (Meinhold *et al.* 2013) was used for the palaeogeographic reconstruction of fragments rifted from Gondwana during Palaeozoic and Mesozoic times. This led to the division of the North African margin of Gondwana, on the basis of zircon age data from Cambrian sandstones, into two separate domains comprising an eastern domain containing 1.0 Ga detrital zircons and a western domain practically devoid of *c.* 1.0 Ga detrital zircons (Meinhold *et al.* 2013). The age population of 1.0 Ga, which is rare in western North Africa (Algeria, Morocco), is more common in the east (Libya, Israel, Jordan), where it was supplied with detritus from the Transgondwanan Supermountain via the Gondwana superfan system (Squire *et al.* 2006; Meinhold *et al.* 2013; Neubauer, 2014).

In summary, it can be concluded that the Neoproterozoic detrital zircons from the studied schist samples of the SSMZ could have their origin in the Arabian-Nubian shield. In the further

discussion, we examine potential relationships to blocks further east, particularly to the South China block.

The South China block was formed by amalgamation of the Yangtze and Cathaysia blocks at *c.* 0.85 Ga, followed by anorogenic, rift-related magmatism at *c.* 820–740 Ma, centring around 850, 820, 800, 780 and 750 Ma, that are coeval with the break-up of the Rodinia supercontinent (e.g. Li *et al.* 2008; Li *et al.* 2009, 2014; Yao *et al.* 2014; Shu *et al.* 2021). As suggested by Yao *et al.* (2014; Fig. 9) and discussed in detail by Li *et al.* (2014), the South China block was most likely an integral part of Gondwanaland during early Palaeozoic time, which matches the palaeomagnetic analysis (Zhang, 2004) and recent plate tectonic reconstructions (Merdith *et al.* 2021). Available geological data shows that the South China block has a great affinity with India or Australia. However, the exact position of the South China block in Gondwana has not been well constrained. For instance, detrital zircon age patterns indicate that the South China block was either adjacent to northern India (Li *et al.* 2014; Yao *et al.* 2014) or between India and Australia (Yu *et al.* 2008; Wang *et al.* 2010; Duan *et al.* 2011; Cawood *et al.* 2013). Furthermore, the presence of the *c.* 533 Ma metamorphic event documented in the hornblende in Cathaysia indicates that the South China block preserves the record of a major Pan-African orogeny, supporting the South China block being an integral part of the Gondwana assembly (Li *et al.* 2017). More significantly, it can help to constrain the location of the South China block in Gondwana, suggesting that the South China block (together with Indochina) was most likely connected to northern India by a ‘Pan-African’ collisional orogeny (Li *et al.* 2014). Recently, Yang *et al.* (2020) found pronounced Neoproterozoic and Cambrian detrital zircon age populations from Ediacaran to Cambrian sandstones of the South China block and interpreted these as evidence for amalgamation and collision of the South China block with Gondwana. These authors also noted the similarity of the South block patterns to those of Iran (Fig. 9).

Taken together, the Arabian–Nubian shield is often referred to as the greatest potential source for the major Precambrian–Palaeozoic detrital zircons in the Iranian microcontinent (e.g. Moghadam *et al.* 2017; Zoleikhaei *et al.* 2020). However, we note that the Iranian microcontinent and South China block may have been geographically close, sharing a similar palaeoenvironment on the northern Gondwana margin.

**6.b.2.b. Palaeobiogeographic arguments.** The late Neoproterozoic to early Palaeozoic palaeobiogeographic patterns provide further important constraints on the relative position of the Iranian microcontinent on the northern Gondwana margin. As mentioned before, the SSMZ, Central Iran and (southern and central) Alborz are considered to have been part of the Iranian microcontinent with the Palaeotethys Ocean in the north and the Neotethys Ocean in the south during late Palaeozoic to Mesozoic times. They bear similar upper Ediacaran to Ordovician, Permian and Triassic strata (Hassanzadeh & Wernicke, 2016). We give details in the following discussion of two scenarios, the classical one (based on Torsvik, 1998; Fig. 10a) and an alternative scenario, in which the South China block is attached to Gondwana, according to the recent findings of Yang *et al.* (2020; Fig. 10b), but on the same latitude.

The principal terranes that are confirmed or commonly assumed to be placed close to the northeastern to northern margin of Gondwana in early Palaeozoic time include the SSMZ, Alborz

and Central Iran terranes of Iran, as well as the Central Afghan terranes and part of the Pamirs, Qiangtang, Lhasa and the Tibetan Himalaya of the Tibetan Plateau, and Sibumasu in south-east Asia (e.g. Stern, 1994; Torsvik & Cocks, 2013; Yao *et al.* 2014; Domeier, 2018). In regard to most palaeogeographic reconstructions, a position of the South China block within the tropical zone of western Gondwana during early Cambrian time is indicated (Kirschvink, 1992; McKerrow *et al.* 1992). Biogeographic studies of the lower Cambrian on the Yangtze Platform of the South China block indicate close relationships with regions of the western margin of Gondwana, in particular with the Tarim Platform, India and Iran and less similarities to Kazakhstan, Australia and parts of West Avalonia (Steiner *et al.* 2007).

The palaeogeographic evidence of the Toyonian archaeocyathan reefs in the Alborz Mountains indicates the first record of metazoan reefs in the Toyonian (Cambrian Stage 4) of Iran and adjacent countries (Lasemi & Amin-Rasouli, 2007). Metazoan reefs spread along the northern margin of Gondwana, arguing for a common Gondwanan margin, and worldwide, such as Siberia, eastern Canada and Nevada, through the rest of early Cambrian time (e.g. James & Kobluk, 1978; James *et al.* 1988; Rowland & Gangloff, 1988; Rowland & Shapiro, 2002).

Hamdi *et al.* (1995) suggested that the middle and upper Cambrian reefs in the Mila Formation of the Alborz Mountains contain a similar sponge genus to that found in the lower middle Cambrian of Australia, the Yangtze Platform in the South China block and the Siberian Platform. Kruse & Zhuravlev (2008) elaborated on this hypothesis by suggesting that the Iranian microcontinent was located along the ‘western’ Gondwana margin adjacent to other central and SE Asian fragments, Arabia, Tibet, India and South China.

More recently, Shahkarami *et al.* (2017a,b) outlined four ichnozones for the clastic sediments of the Soltanieh Formation in the central Alborz Mountains, indicating continuous sedimentation from Ediacaran through Cambrian times. These authors argued that ichnozone 1 in the Alborz Mountains is evidenced by the *Treptichnus pedum* zone, which is the index fossil for the lowermost Cambrian. This reveals a similar situation for the Ediacaran–Cambrian succession of the Alborz Mountains and eastern Yunnan Province, South China (Zhu, 1997), western Mongolia (Smith *et al.* 2015), Lesser Himalaya, India (Singh *et al.* 2014) and southern Kazakhstan (Weber *et al.* 2013), where the first appearance of the trace fossil *T. pedum* post-dates the Ediacaran–Cambrian transition. Similarly, Hamdi *et al.* (1989) found evidence of an assemblage of phosphatic layers in the Lower Shale Member in the Alborz Mountains and pointed out the similarities with successions containing a major Tommotian phosphorite horizon nearly contemporaneous across the ‘Proto-/Palaeotethyan’ belt in South China, India, Pakistan, Kazakhstan and Mongolia.

The new late Cambrian species of Siphonotretida recognized in the Alborz is the only known Cambrian representative of the group with distinct characteristics (Popov *et al.* 2009a), different from other siphonotretide genera, e.g. on both sides of the Iapetus Ocean in Laurentia and Gondwana (Armorica), and in west Antarctica (Shergold *et al.* 1976; Popov *et al.* 2002; González-Cómez, 2005). The unique features of the late Cambrian Siphonotretida of Iran are also characteristics of most of the Ordovician siphonotretide genera, which likely were rooted originally in high to temperate latitudes of peri-Gondwana (Fig. 10; Havlíček, 1982; Mergl, 2002; Popov *et al.* 2008). Popov *et al.*

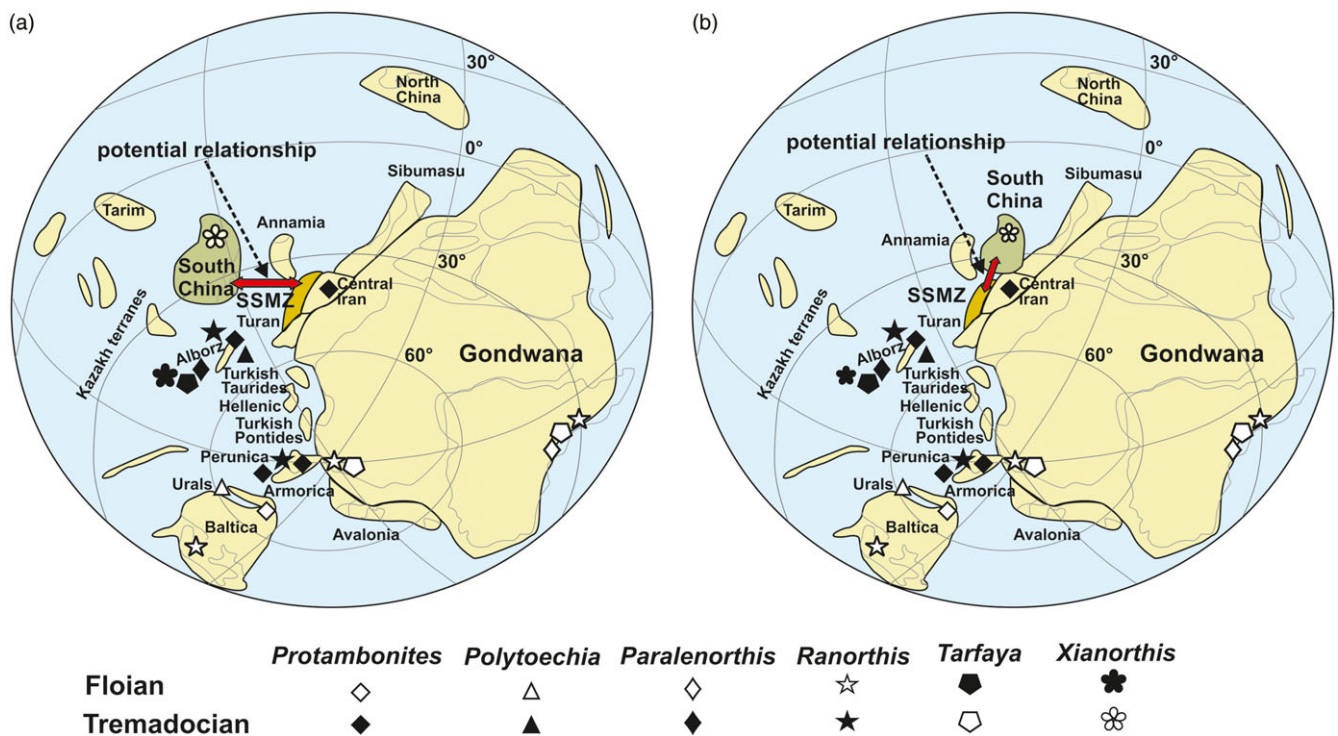


**Fig. 10.** (Colour online) (a) Palaeogeographic reconstruction for the late Tremadocian–Floian stages showing the geographic distribution of rhynchonelliform brachiopod genera (from Popov *et al.* 2009a, based on Torsvik, 1998), which occur in the lower part of the Lashkarak Formation (modified from Torsvik, 1998 and Ghobadi Pour, 2006). Note the potential close neighbourhood of South China and Central Iran/SSMZ at similar latitudes assuming that the units could be freely shifted along latitudes (because of the undetermined longitude). (b) This reconstruction according to Yang *et al.* (2020) puts the South China block in East Gondwana. Red double arrow indicates the palaeobiogeographic relationships.

(2013) suggested that it can be typified by those described from the Middle Ordovician of Baltica (Gorjansky, 1969; Holmer, 1989) and South China (Zhang, 1995).

Dong *et al.* (2004) discussed 13 middle Cambrian through lowermost Ordovician conodont zones in Hunan, South China and their similarities with Iran (Müller, 1973) and correlated these with North China, western USA, western Newfoundland and Canada. In addition, the Early–Middle Ordovician palaeobiogeographic patterns of the brachiopod faunas from the Upper Yangtze Platform, South China were documented (Zhan & Jin, 2014), indicating a close faunal relationship between South China and Iran (Popov *et al.* 2009b).

The Lower Ordovician (Tremadocian) trilobite assemblage, as well as Darriwilian brachiopods in the Alborz, exhibit a close similarity to contemporaneous trilobite faunas of South China (e.g. Ghobadi Pour, 2006; Ghobadi Pour *et al.* 2007, 2011; Álvaro *et al.* 2013; Kebria-ee Zadeh *et al.* 2015). Ghobadi Pour *et al.* (2007) noted the species *Taihungshania miqueli* (Bergeron, 1894), the third diagnosable species, which has been recorded from South China, Turkey and Southern France, indicating North Gondwanan faunal affinities. In the eastern Alborz (Gerd-Kuh section), the lower Tremadocian *Asaphellus inflatus*–*Dactylocephalus* and *Psiloccephalina lubrica* zones are characterized by medium diversity trilobite associations with strong links to contemporaneous faunas of South China (Ghobadi Pour *et al.* 2015b). In addition, abundant and diverse brachiopods are present throughout the Gerd-Kuh section, and, as Popov & Cocks (2017) pointed out, Alborz is one of the few places globally which has a strophomenoid-dominated benthic assemblage in the Middle Ordovician brachiopod fauna, providing the opportunity to investigate the

palaeogeographic and climatic control on their initial divergence. These authors suggested that the Australasian (Sibumasu) sector of Gondwana was the primary location of the origin and initial dispersion of the Strophomenoidea, as well as the adjacent terranes and satellite plates of peri-Gondwana, including Alborz, North China and South China (Popov & Cocks, 2017).

The first occurrence of Late Ordovician trilobites from the High Zagros, has been reported in the middle member of the Seyahou Formation (Ghobadi Pour *et al.* 2015a). This formation hosts a trilobite assemblage including *Dalmanitina (Dalmanitina) dargazensis*, which shows strong affinities with high-to-mid-latitude peri-Gondwanan faunas, and displays close similarities with taxa from the Mediterranean margin of Gondwana (mainly Sardinia and Bohemia/Perunica) and, to a lesser extent, with the Turkish Taurides (Ghobadi Pour *et al.* 2015a).

Ameri (2015) reported a peri-Gondwanan trilobite assemblage from the Kuhbanan Formation at Dahu, north Kerman, which is the most complete fossiliferous upper lower Cambrian – middle Cambrian sequence in Central Iran. The distribution of the Kuhbanan Formation trilobite species (*Redlichia* Biozone) shows close faunal connections to the Hormoz Formation from South and SW Iran, the Salt Range (Pakistan), the Himalayan region, southern Siberia, Australia and South China (Ameri, 2015).

Popov *et al.* (2014) reported an important record of biotic recovery of benthic faunas in the Llandovery deposits of Iran after the terminal Ordovician mass extinction in temperate and high latitude Gondwana, which is still poorly known in the Mediterranean, North African and Arabian segments of Gondwana. A significant number of taxa from the shallow shelf biofacies indicates clear links to contemporaneous low-latitude faunas, for instance to Laurentia,

540 Ma

TPW Reconstruction

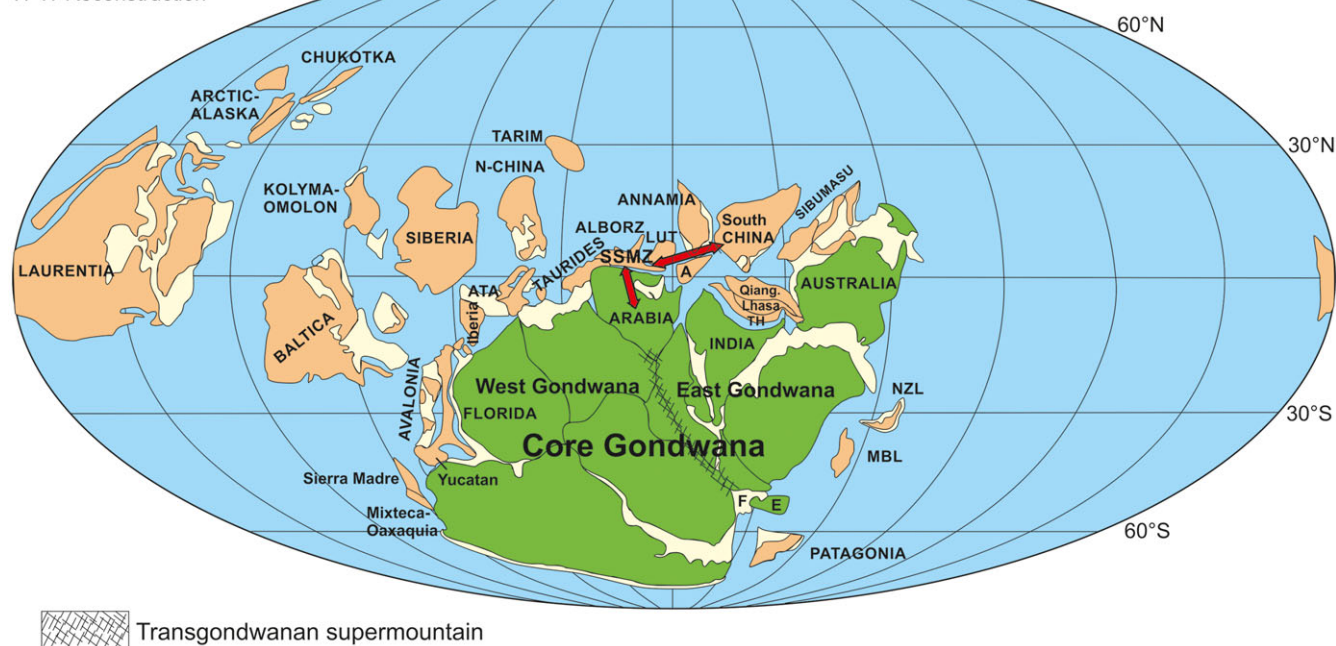


**Fig. 11.** (Colour online) Global reconstruction for the earliest Cambrian (540 Ma), showing the location along Gondwana of the blocks (modified after Torsvik & Cocks, 2013 and Yao *et al.* 2014). The red arrows point to the biogeographic and detrital zircon provenance relationships in the reconstruction. West and East Gondwana are separated by the Transgondwanan Supermountain. A – Afghan Terrane; ATA – Armorican Terrane Assemblage; E – Ellsworth-Whitmore Mountains; F – Falkland Islands; MBL – Marie Byrd Land; NZL – New Zealand; Qiang. – Qiantang Terrane; SSMZ – Sanandaj–Sirjan metamorphic zone; TH – Tethyan Himalaya.

Baltica and South China (Popov *et al.* 2014). The authors proposed the close proximity of the peri-Gondwanan terranes of Central Iran, Kopet Dagh and Afghanistan, owing to the bearing of shallow water faunas during the Aeronian of the Silurian period.

In summary, late Neoproterozoic to the early Silurian faunas, restricted to the same type of palaeoenvironment, are shared by the Iranian microcontinent and South China block and represent key elements to determine their palaeogeographic similarities along the Gondwanan margin (Figs 10, 11). Li *et al.* (2014) and Yang *et al.* (2020) proposed that the South China block was accreted to East Gondwana during late Neoproterozoic–Cambrian times. Consequently, the Iranian microcontinent including the SSMZ can be considered as being part of the same Cambrian–early Silurian Gondwanan margin. Comparison of detrital zircons show similar age patterns in terranes originating from north of the Arabian–Nubian shield via the Iranian microcontinent to far in the east, along the northern Gondwana margin (Fig. 11).

## 7. Conclusions

New detrital U–Pb zircon ages from the SSMZ provide new insights into the palaeogeographic reconstruction of the Iranian microcontinent. Our conclusions are summarized as follows:

(1) The youngest peak and weighted mean ages in the probability diagrams provide geochronological maximum depositional ages for hitherto undated metamorphic units. In particular, detrital zircon ages from the younger garnet–micaschist sample (GQ-12) represent a maximum depositional age of the

sediments not older than latest Triassic, consistent with the metamorphosed Jurassic sediments widespread within the central SSMZ.

- (2) The reproducibility is remarkable of the age population peak at *c.* 0.6 Ga, which represents a distinct signal related to the late Neoproterozoic crystalline basement in Iran as well as to the Arabian–Nubian shield and other Pan-African domains in northern Gondwana. The other significant Neoproterozoic age populations in all three samples likely derived from magmatic rocks and/or recycled sedimentary sources, possibly from the eastern Arabian–Nubian shield.
- (3) New zircon age data from garnet–micaschists demonstrates the presence of a late Grenvillian age population at *c.* 0.94 to 1.1 Ga within the SSMZ, which led to deducing the proximity of the Sanandaj–Sirjan zone to distal parts of the ‘Gondwana superfan’ at the northern margins of Gondwana. The Grenvillian detrital age population suggests that the ‘Gondwana superfan’ even spread detrital material far east along the northern Gondwana margin and reached the South China block, where this age group occurs but remains subordinate (e.g. Yang *et al.* 2020).
- (4) It is worth noting that further research should focus on more detrital zircon ages from metamorphic clastic rocks and Cambrian–Ordovician sandstones as well as obtaining the biogeographic distribution of Cambrian–Ordovician shallow marine organisms that would also provide better insights into the palaeogeographic reconstruction of the northern Gondwana margin during early Palaeozoic time.

**Supplementary material.** To view supplementary material for this article, please visit <https://doi.org/10.1017/S0016756821000728>

**Acknowledgements.** We gratefully acknowledge constructive comments and suggestions from two anonymous reviewers, which helped to clarify ideas and content. We also thank the editor, Olivier Lacombe, for his encouragement. Farzaneh Shakerardakani acknowledges support via a scholarship from the Afro-Asiatisches Institut Salzburg for her Ph.D. thesis at the Salzburg University, and a PIFI postdoctoral fellowship from the Chinese Academy of Sciences. This study was financially supported by the Strategic Priority Research Programme (B) of the Chinese Academy of Sciences (XDB18030300) to XHL.

## References

- Abbo A, Avigad D, Gerdes A and Güngör T** (2015) Cadomian basement and Paleozoic to Triassic siliciclastics of the Taurides (Karacahisar dome, south-central Turkey): paleogeographic constraints from U–Pb–Hf in zircons. *Lithos* **227**, 122–39.
- Abbo A, Avigad D, Gerdes A, Morag N and Vainer S** (2020) Cadomian (ca. 550 Ma) magmatic and thermal imprint on the North Arabian–Nubian Shield (south and central Israel): new age and isotopic constraints. *Precambrian Research* **346**, 105804. doi: [10.1016/j.precamres.2020.105804](https://doi.org/10.1016/j.precamres.2020.105804).
- Abd El-Rahman Y, Abu Anbar M, Li XH, Li J, Ling XX, Wu LG and Masoud AE** (2019) The evolution of the Arabian–Nubian Shield and survival of its zircon U–Pb–Hf–O isotopic signature: a tale from the Um Had Conglomerate, central Eastern Desert, Egypt. *Precambrian Research* **320**, 46–62.
- Agard P, Omrani J, Jolivet L, Whitchurch H, Vrielynck B, Spakman W, Monie P, Meyer B and Wortel R** (2011) Zagros orogeny: a subduction-dominated process. *Geological Magazine* **148**, 692–725.
- Alavi M** (1994) Tectonics of the Zagros orogenic belt of Iran: new data and interpretations. *Tectonophysics* **229**, 211–38.
- Alavi M and Bolourchi MH** (1973) Explanatory Text of the Maku Quadrangle Map 1:250 000. Geological Quadrangle, A1. Tehran: Geological Survey of Iran, 44 pp.
- Alavi-Naini M** (2009) *Stratigraphy of Iran*. Tehran: Geological Survey of Iran, 507 pp. (in Persian)
- Ali BH, Wilde SA and Gabr MMA** (2009) Granitoid evolution in Sinai, Egypt, based on precise SHRIMP U–Pb zircon geochronology. *Gondwana Research* **15**, 38–48.
- Ali KA, Jeon H, Andresen A, Li SQ, Harbi HM and Hegner E** (2014) U–Pb zircon geochronology and Nd–Hf–O isotopic systematics of the Neoproterozoic Hadb adh Dayheen ring complex, Central Arabian Shield, Saudi Arabia. *Lithos* **206–207**, 348–60.
- Ali KA, Kröner A, Hener E, Wong J, Li SQ, Gahlan HA and Abu El Ela FF** (2015) U–Pb zircon geochronology and Hf–Nd isotopic systematics of Wadi Beitan granitoid gneisses, South Eastern Desert, Egypt. *Gondwana Research* **27**, 811–24.
- Ali KA, Stern RJ, Manton WI, Johnson PR and Mukherjee SK** (2010) Neoproterozoic diamicite in the Eastern Desert of Egypt and Northern Saudi Arabia: evidence of ~750 Ma glaciation in the Arabian–Nubian Shield. *International Journal of Earth Sciences* **90**, 705–26.
- Ali KA, Stern RJ, Manton WI, Kimura JI and Khamees H** (2009) Geochemistry, Nd isotopes and U–Pb SHRIMP zircon dating of Neoproterozoic volcanic rocks from the Central Eastern Desert of Egypt: new insights into the ~750 Ma crust-forming event. *Precambrian Research* **171**, 1–22.
- Alirezai S and Hassanzadeh J** (2012) Geochemistry and zircon geochronology of the Permian A-type Hasanrobat granite, Sanandaj–Sirjan belt: a new record of the Gondwana break-up in Iran. *Lithos* **151**, 122–34.
- Álvoro JJ, Ahlberg P, Babcock LE, Bordonaro OL, Choi DK, Cooper RA, Ergaliev GKH, Gapp IW, Ghobadi Pour M, Hughes NC, Jago JB, Korovnikov I, Laurie JR, Lieberman BS, Paterson JR, Pegel TV, Popov LE, Rushton AWA, Sukhov S, Tortello MF, Zhou Z and Žylińska A** (2013) Global Cambrian trilobite palaeobiogeography assessed using parsimony analysis of endemicity. In *Early Palaeozoic Biogeography and Palaeogeography* (eds DAT Harper and T Servais), pp. 273–96. Geological Society of London, Memoirs no. 38.
- Ameri H** (2015) Peri-Gondwana Late Early–Middle Cambrian trilobites from the Kuhbanan Formation in Dahu section, Kerman Province, Iran. *Arabian Journal of Geosciences* **8**, 1467–78.
- Andersen A, El-Rus MMA, Myhre PI, Boghdady GY and Corfu F** (2009) U–Pb TIMS age constraints on the evolution of the Neoproterozoic Meatiq Gneiss Dome, Eastern Desert, Egypt. *International Journal of Earth Sciences* **98**, 481–97.
- Andersen T** (2002) Correction of common lead in U–Pb analyses that do not report <sup>204</sup>Pb. *Chemical Geology* **192**, 59–79.
- Assereto R** (1963) The Paleozoic formations in central Elburz (Iran) (preliminary note). *Rivista Italiana di Paleontologia e Stratigrafia* **69**, 503–43.
- Augland LE, Andresen A and Boghdady GY** (2012) U–Pb ID–TIMS dating of igneous and metagneous rocks from the El-Sibai area: time constraints on tectonic evolution of the Central Eastern Desert, Egypt. *International Journal of Earth Sciences* **101**, 25–37.
- Avigad D, Kolodner K, McWilliams M, Persing H and Weissbrod T** (2003) Origin of northern Gondwana Cambrian sandstone revealed by detrital zircon SHRIMP dating. *Geology* **31**, 227–30.
- Avigad D, Morag N, Abbo A and Gerdes A** (2017) Detrital rutile U–Pb perspective on the origin of the great Cambro–Ordovician sandstone of North Gondwana and its linkage to orogeny. *Gondwana Research* **51**, 17–29.
- Avigad D, Weissbrod T, Gerdes A, Zlatkin, O, Ireland TR and Morag N** (2015) The detrital zircon U–Pb–Hf fingerprint of the northern Arabian–Nubian Shield as reflected by a Late Ediacaran arkosic wedge (Zenifim Formation; subsurface Israel). *Precambrian Research* **266**, 1–11.
- Bagheri S and Stampfli GM** (2008) The Anarak, Jandaq and Posht-e-Badam metamorphic complexes in central Iran: new geological data, relationships and tectonic implications. *Tectonophysics* **451**, 123–55.
- Be’eri-Shlevin Y, Eyal M, Eyal Y, Whitehouse MJ and Litvinovsky B** (2012) The Sa’al volcano-sedimentary complex (Sinai, Egypt), a latest Mesoproterozoic volcanic arc in the northern Arabian Nubian Shield. *Geology* **40**, 403–6.
- Be’eri-Shlevin Y, Katzir Y and Whitehouse MJ** (2009) Post-collisional tectono-magmatic evolution in the northern Arabian Nubian Shield (ANS): time constraints from ionprobe U–Pb dating of zircon. *Journal of the Geological Society, London* **166**, 1–15.
- Bea F, Mazhari A, Montero P, Amini S and Ghalamghash J** (2011) Zircon dating, Sr and Nd isotopes, and element geochemistry of the Khalifan pluton, NW Iran: evidence for Variscan magmatism in a supposedly Cimmerian superterrane. *Journal of Asian Earth Science* **44**, 172–9.
- Bea R, Abu-Anbar N, Montero P, Peres P and Talavera C** (2009) The ~844 Ma Moneiga quartz-diorites of the Sinai, Egypt: evidence for Andean-type arc or rift-related magmatism in the Arabian–Nubian Shield? *Precambrian Research* **175**, 161–8.
- Belousova EA, Griffin WL, O’Reilly SY and Fisher NI** (2002) Igneous zircon: trace element composition as an indicator of host rock type. *Contributions to Mineralogy and Petrology* **143**, 602–22.
- Berberian M and King GCP** (1981) Towards a paleogeography and tectonic evolution of Iran. *Canadian Journal of Earth Sciences* **18**, 210–65.
- Bergeron J** (1894) Notes paléontologiques I. Crustacés. *Bulletin de la Société géologique de France* **21** (for 1893), 333–46.
- Black LP, Kamo SL, Allen CM, Aleinikoff JN, Davis DW, Korsch RJ and Foudoulis C** (2003) TEMORA 1: a new zircon standard for Phanerozoic U–Pb geochronology. *Chemical Geology* **200**, 155–70.
- Buchs DM, Bagheri S, Martin L, Hermann J and Arculus R** (2013) Paleozoic to Triassic ocean opening and closure preserved in Central Iran: constraints from the geochemistry of meta-igneous rocks of the Anarak area. *Lithos* **172–173**, 267–87.
- Cawood PA, Wang Y, Xu Y and Zhao G** (2013) Locating South China in Rodinia and Gondwana: a fragment of greater India lithosphere? *Geology* **41**, 903–6.
- Charvet J** (2013) The Neoproterozoic–Early Paleozoic tectonic evolution of the South China Block: an overview. *Journal of Asian Earth Sciences* **74**, 198–209.
- Cohen KM, Finney SC, Gibbard PL and Fan J-X** (2013) The ICS International Chronostratigraphic Chart. *Episodes* **36**, 199–204.
- Collins AS and Pisarevsky SA** (2005) Amalgamating eastern Gondwana: the evolution of the Circum-Indian Orogens. *Earth-Science Reviews* **71**, 229–70.

- Compston W, Zhang Z, Cooper JA, Ma GG and Jenkins RJF** (2008) Further SHRIMP geochronology on the early Cambrian of south China. *American Journal of Sciences* **308**, 399–420.
- Condon D, Zhu MY, Bowring S, Wang W, Yang AH and Jin YG** (2005) U–Pb ages from the Neoproterozoic Doushantuo Formation, China. *Science* **308**, 95–8.
- Corfu F** (2004) U–Pb age, setting and tectonic significance of the anorthosite-mangerite-harnockite-granite suite, Lofoten–Vesteralen, Norway. *Journal of Petrology* **45**, 1799–819.
- Corfu F, Hanchar JM, Hoskin PWO and Kinny P** (2003) Atlas of zircon textures. *Reviews in Mineralogy and Geochemistry* **53**, 469–500.
- Cox GM, Foden J and Collins A** (2019) Late Neoproterozoic adakitic magmatism of the eastern Arabian Nubian Shield. *Geoscience Frontiers* **10**, 1981–92.
- Davoudian AR, Genser J, Neubauer F and Shabanian N** (2016)  $^{40}\text{Ar}$ – $^{39}\text{Ar}$  mineral ages of eclogite from North Shahrekord in the Sanandaj–Sirjan Zone, Iran: implications for the tectonic evolution of Zagros orogen. *Gondwana Research* **37**, 216–40.
- Derakhshi M and Ghasemi H** (2015) Soltan Maidan Complex (SMC) in the eastern Alborz structural zone, northern Iran: magmatic evidence for Paleotethys development. *Arabian Journal of Geosciences* **8**, 849–66.
- Dickinson WR and Gehrels GE** (2009) Use of U–Pb ages of detrital zircons to infer maximum depositional ages of strata: a test against a Colorado Plateau Mesozoic database. *Earth and Planetary Science Letters* **288**, 115–25.
- Domeier M** (2018) Early Paleozoic tectonics of Asia: towards a full-plate model. *Geoscience Frontiers* **9**, 789–862.
- Dong XP, Repetski JE and Bergström SM** (2004) Conodont biostratigraphy of the Middle Cambrian through lowermost Ordovician in Hunan, South China. *Acta Geologica Sinica* **78**, 1185–206.
- Dong YP, Liu XM, Santosh M, Chen Q, Zhang XN, Li W, He DF and Zhang GW** (2012) Neoproterozoic accretionary tectonics along the northwestern margin of the Yangtze Block, China: constraints from zircon U–Pb geochronology and geochemistry. *Precambrian Research* **196–197**, 247–74.
- Du LL, Guo JH, Nutman AP, Wyman D, Geng YS, Yang CH, Liu FL, Ren LD and Zhou XW** (2014) Implications for Rodinia reconstructions for the initiation of Neoproterozoic subduction at similar to 860 Ma on the western margin of the Yangtze Block: evidence from the Guandaoshan Pluton. *Lithos* **196**, 67–82.
- Duan L, Meng QR, Zhang CL and Liu XM** (2011) Tracing the position of the South China block in Gondwana: U–Pb ages and Hf isotopes of Devonian detrital zircons. *Gondwana Research* **19**, 141–9.
- Etemad-Saeed N, Hosseini-Barzi M, Adabi M, Miller NR, Sadeghi A, Houshmandzadeh A and Stockli DF** (2015) Evidence for ca. 560 Ma Ediacaran glaciation in the Kahar Formation, central Alborz Mountains, northern Iran. *Gondwana Research* **31**, 164–83.
- Falcon NL** (1974) Southern Iran: Zagros Mountains. In *Mesozoic–Cenozoic Orogenic Belts: Data for Orogenic Studies* (ed. AM Spencer), pp. 199–211. Geological Society of London, Special Publication no. 4.
- Fazlnia A, Moradian A, Rezaei K, Moazzen M and Alipour S** (2007) Synchronous activity of anorthositic and S-type granitic magmas in Chah–Dozdan batholite, Neyriz, Iran: evidence of zircon SHRIMP and monazite CHIME dating. *Journal of Sciences, Islamic Republic of Iran* **18**, 221–37.
- Fergusson CL, Nutman AP, Mohajjel M and Bennett V** (2016) The Sanandaj–Sirjan zone in the Neo-Tethyan suture, western Iran: zircon U–Pb evidence of late Palaeozoic rifting of northern Gondwana and mid-Jurassic orogenesis. *Gondwana Research* **40**, 43–57.
- Gehrels GE** (2014) Detrital zircon U–Pb geochronology applied to tectonics. *Annual Review of Earth and Planetary Sciences* **42**, 127–49.
- Ghanem H, McAleer RJ, Jarrar G, Hseinat M and Whitehouse M** (2020)  $^{40}\text{Ar}$ / $^{39}\text{Ar}$  and U–Pb SIMS zircon ages of Ediacaran dikes from the Arabian–Nubian Shield of south Jordan. *Precambrian Research* **343**, 105714. doi: [10.1016/j.precamres.2020.105714](https://doi.org/10.1016/j.precamres.2020.105714).
- Ghasemi H and Dayhimi M** (2015) Devonian alkaline basic magmatism in Eastern Alborz, north of Shahrood: evidence for Paleotethys rifting. *Iranian Journal of Geology* **32**, 19–32 (in Persian).
- Ghazi M, Hassanipak AA, Tucker PJ, Mobasher K and Duncan RA** (2001) Geochemistry and  $^{40}\text{Ar}$ – $^{39}\text{Ar}$  ages of the Mashhad Ophiolite, NE Iran: a rare occurrence of a 300 Ma (Paleo-Tethys) oceanic crust. American Geophysical Union, Fall Meeting, Abstract I12C-0993.
- Ghobadi Pour M** (2006) Early Ordovician (Tremadocian) trilobites from Simeh-Kuh, Eastern Alborz, Iran. In *Studies in Palaeozoic Palaeontology* (eds MG Bassett and VK Deisler), pp. 93–118. Cardiff: National Museum of Wales, Geological Series no. 25.
- Ghobadi Pour M, Ghavidel-Syooki M, Álvaro JJ, Popov LE and Ehsani MH** (2015a) First reported Late Ordovician trilobites from the High Zagros Range, Iran: a biogeographic link between Gondwanan Chinese and Mediterranean faunas. *Geobios* **48**, 351–69.
- Ghobadi Pour M, Popov LE, Holmer LE, Hosseini-Nezhad M, Rasuli R, Fallah K, Amini A and Jahangiri H** (2015b) Early Ordovician (Tremadocian) faunas and biostratigraphy of the Gerd-Kuh section, eastern Alborz, Iran. *Stratigraphy* **12**, 55–61.
- Ghobadi Pour M, Popov LE, Kebria-ee Zadeh MR and Baars C** (2011) Middle Ordovician (Darriwilian) brachiopods associated with the *Neseuretus* biofacies, eastern Alborz Mountains, Iran. *Memoirs of the Association of Australian Palaeontologists* **42**, 263–83.
- Ghobadi Pour M, Vidal M and Hosseini-Nezhad M** (2007) An Early Ordovician trilobite assemblage from the Lashkarak Formation, Damghan area, northern Iran. *Geobios* **40**, 489–500.
- González-Gómez C** (2005) Linguliformean brachiopods of the Middle–Upper Cambrian transition from the Val d’Homs Formation, southern Montagne Noire, France. *Journal of Paleontology* **79**, 29–47.
- Gorjansky VY** (1969) Inarticulate brachiopods of the Cambrian and Ordovician of the Northwest Russian Platform. *Ministerstvo Geologii RSFSR, Severo-Zapadnoe Territorialnoe Geologicheskoe Upravlenie* **6**, 1–173 (in Russian).
- Grimes CB, Jhon BE, Kelemen PB, Mazdab FK, Wooden JL, Cheadle MJ, Hanghoj K and Schwartz JJ** (2007) Trace element chemistry of zircons from oceanic crust: a method for distinguishing detrital zircon provenance. *Geology* **35**, 643–6.
- Grimes CB, Wooden JL, Cheadle MJ and John BE** (2015) “Fingerprinting” tectono-magmatic provenance using trace elements in igneous zircon. *Contributions to Mineralogy and Petrology* **170**, 46. doi: [10.1007/s00410-015-1199-3](https://doi.org/10.1007/s00410-015-1199-3).
- Hamdi B, Brasier MD and Zhiwen J** (1989) Earliest skeletal fossils from Precambrian–Cambrian boundary strata, Elburz Mountains, Iran. *Geological Magazine* **126**, 283–9.
- Hamdi B, Rozanov AY and Zhuravlev AY** (1995) Latest Middle Cambrian metazoan reef from northern Iran. *Geological Magazine* **132**, 367–73.
- Hassan M, Stüwe K, Abu-Alam TS, Klötzli U and Tiepolo M** (2016) Time constraints on deformation of the Ajaj branch of one of the largest Proterozoic shear zones on Earth: the Najd Fault System. *Gondwana Research* **34**, 346–62.
- Hassanzadeh J, Stockli DF, Horton BK, Axen GJ, Stockli LD, Grove M, Schmitt AK and Walker JD** (2008) U–Pb zircon geochronology of late Neoproterozoic–Early Cambrian granitoids in Iran: implications for paleogeography, magmatism, and exhumation history of Iranian basement. *Tectonophysics* **451**, 71–96.
- Hassanzadeh J and Wernicke BP** (2016) The Neotethyan Sanandaj–Sirjan zone of Iran as an archetype for passive margin-arc transitions. *Tectonics* **35**, 586–621.
- Havlíček V** (1982) Lingulacea, Paterinacea, and Siphonotretacea (Brachiopoda) in the Lower Ordovician sequence of Bohemia. *Sborník geologických věd. Paleontologie* **25**, 9–82.
- Hedge CE** (1984) Precambrian Geochronology of Part of Northwestern Saudi Arabia, Kingdom of Saudi Arabia. Kingdom of Saudi Arabian Deputy Ministry for Mineral Resources. United States Geological Survey Open-File Report 84-381, 14 pp.
- Holmer LE** (1989) Middle Ordovician phosphatic inarticulate brachiopods from Västergötland and Dalarna, Sweden. *Fossils and Strata* **26**, 1–172.
- Honarmand M, Li XH, Nabatian G and Neubauer F** (2017) In-situ zircon U–Pb age and Hf–O isotopic constraints on the origin of the Hasan-Robat A-type granite from Sanandaj–Sirjan zone, Iran: implications for reworking of Cadomian arc igneous rocks. *Mineralogy and Petrology* **111**, 659–75.
- Honarmand M, Li XH, Nabatian G, Rezaeian M and Etemad-Saeed N** (2016) Neoproterozoic–Early Cambrian tectono-magmatic evolution of the Central

- Iranian terrane, northern margin of Gondwana: constraints from detrital zircon U–Pb and Hf–O isotope studies. *Gondwana Research* **37**, 285–300.
- Horton BK, Hassanzadeh J, Stockli DF, Axen GJ, Gillis RJ, Guest B, Amini AH, Fakhari M, Zamanzadeh SM and Grove M** (2008) Detrital zircon provenance of Neoproterozoic to Cenozoic deposits in Iran: implications for chronostratigraphy and collisional tectonics. *Tectonophysics* **451**, 97–122.
- Hoskin PWO and Ireland TR** (2000) Rare earth element chemistry of zircon and its use as a provenance indicator. *Geology* **28**, 627–30.
- Hoskin PWO and Schaltegger U** (2003) The composition of zircon and igneous and metamorphic petrogenesis. *Reviews in Mineralogy and Geochemistry* **53**, 25–104.
- Houshmandzadeh A, Soheile M and Hamdi B** (1990) Explanatory Text of the Eqolid Quadrangle Map 1:25000. Geological Quadrangle, No. G 10. Tehran: Geological Survey of Iran, Ministry of Mines and Metals.
- James NP and Kobluk DR** (1978) Lower Cambrian patch reefs and associated sediments, Southern Canada. *Sedimentology* **25**, 1–35.
- James NP, Kobluk DR and Klapa CF** (1988) Early Cambrian patch reefs, Southern Labrador. In *Reefs, Canada and Adjacent Area* (eds HHJ Geldsetzer, NP James and GE Tebbutt), pp. 141–50. Canadian Society of Petroleum Geologist Memoir 13.
- Jamshidi Badr M, Collins AS, Masoudi F, Cox G and Mohajjel M** (2013) The U–Pb age, geochemistry and tectonic significance of granitoids in the Soursat Complex, Northwest Iran. *Turkish Journal of Earth Sciences* **22**, 1–31. doi: [10.3906/yer-1001-37](https://doi.org/10.3906/yer-1001-37).
- Johnson PR, Andersen A, Collins AS, Fowler AR, Fritz H, Ghebreab W, Kusky T and Stern RJ** (2011) Late Cryogenian–Ediacaran history of the Arabian–Nubian Shield: a review of depositional, plutonic, structural, and tectonic events in the closing stages of the northern East African Orogen. *Journal of African Earth Sciences* **10**, 1–179.
- Johnson PR, Halverson GP, Kusky TM, Stern RJ and Pease V** (2013) Volcanosedimentary basins in the Arabian–Nubian Shield: markers of repeated exhumation and denudation in a Neoproterozoic accretionary orogen. *Geosciences* **3**, 389–445.
- Kargaranbafghi F, Neubauer F and Genser J** (2015) The tectonic evolution of western Central Iran seen through detrital white mica. *Tectonophysics* **651–652**, 138–51.
- Kebriaee Zadeh MR, Ghobadi Pour M, Popov LE, Baars CH and Jahangiri H** (2015) First record of the Ordovician fauna in Mila-Kuh, eastern Alborz, northern Iran. *Estonian Journal of Earth Sciences* **64**, 121–39.
- Kennedy A, Kozdrój W, Johnson PR and Kattan FH** (2011a) SHRIMP Geochronology in the Northern Arabian Shield. Part III. Data Acquisition 2006. Saudi Geological Survey Open-File Report SGS-OF-2007-9, 85 pp.
- Kennedy A, Kozdrój W, Kadi K, Kozdrój MZ and Johnson PR** (2011b) SHRIMP Geochronology in the Arabian Shield (Midyan Terrane, Afif Terrane) and Nubian Shield (Central Eastern Desert Terrane), Part V: Data Acquisition 2009. Saudi Geological Survey. Open-File Report SGS-OF-2010-11, 80 pp.
- Kennedy A, Kozdrój W, Kattan FH, Kozdrój MZ and Johnson PR** (2010) SHRIMP Geochronology in the Arabian Shield (Midyan Terrane, Afif Terrane, Ad Dawadimi Terrane) and Nubian Shield (Central Eastern Desert), Part IV: Data Acquisition 2008. Saudi Geological Survey Open-File Report SGS-OF-2010-10, 101 pp.
- Khudeir AA, Paquette JL, Nicholson K, Johansson Å, Rooney TO, Hamdi S, El-Fadly MA, Corcoran L, Malone SJ and El-Rus MAA** (2021) On the cratonization of the Arabian–Nubian Shield: constraints from gneissic granitoids in south Eastern Desert, Egypt. *Geoscience Frontiers* **12**, 101148. doi: [10.1016/j.gsf.2021.101148](https://doi.org/10.1016/j.gsf.2021.101148).
- Kirschvink JL** (1992) A paleogeographic model for Vendian and Cambrian time. In *The Proterozoic Biosphere: A Multidisciplinary Study* (eds JW Schopf, C Klein and DD Maris), pp. 567–81. Cambridge: Cambridge University Press.
- Kolodner K, Avigad D, McWilliams M, Wooden JL, Weissbrod T and Feinstein S** (2006) Provenance of north Gondwana Cambrian–Ordovician sandstone: U–Pb SHRIMP dating of detrital zircons from Israel and Jordan. *Geological Magazine* **143**, 367–91.
- Kozdrój W, Kennedy AK, Johnson PR, Ziolkowska-Kozdrój M and Kadi K** (2018) Geochronology in the southern Midyan terrane: a review of constraints on the timing of magmatic pulses and tectonic evolution in a northwestern part of the Arabian Shield. *International Geology Review* **60**, 1290–319.
- Kruse PD and Zhuravlev AY** (2008) Middle-Late Cambrian *Rankenella-Girvanella* reefs of the Mila Formation, northern Iran. *Canadian Journal of Earth Sciences* **45**, 619–39.
- Lammerer B, Langheinrich G and Manutchehr-Daini M** (1984) Geological investigations in the Binalud Mountains (NE Iran). *Neues Jahrbuch für Geologie und Paläontologie, Abhandlungen* **168**, 269–77.
- Lan ZW, Li XH, Chu X, Tang G, Yang S, Yang H, Liu H, Jiang T and Wang T** (2017) SIMS U–Pb zircon ages and Ni–Mo–PGE geochemistry of the lower Cambrian Niutitang Formation in South China: constraints on Ni–Mo–PGE mineralization and stratigraphic correlations. *Journal of Asian Earth Sciences* **137**, 141–62.
- Lan ZW, Li XH, Zhu MY, Zhang QR and Li QL** (2015) Revisiting the Liantuo Formation in Yangtze Block, South China: SIMS U–Pb zircon age constraints and regional and global significance. *Precambrian Research* **263**, 123–41.
- Lasemi Y and Amin-Rasouli H** (2007) Archaeocyathan buildups within an entirely siliciclastic succession: new discovery in the Toyonian Lalun Formation of northern Iran, the Proto-Paleotethys passive margin of northern Gondwana. *Sedimentary Geology* **201**, 302–20.
- Li L, Lin S, Xing G, Jiang Y and He J** (2017) First direct evidence of Pan-African orogeny associated with Gondwana assembly in the Cathaysia Block of Southern China. *Scientific Reports* **7**, 794. doi: [10.1038/s41598-017-00950-x](https://doi.org/10.1038/s41598-017-00950-x).
- Li XH, Abd El-Rahman Y, Abu Anbar M, Li J, Ling XX, Wu LG and Masoud AE** (2018) Old continental crust underlying juvenile oceanic arc: evidence from northern Arabian–Nubian Shield, Egypt. *Geophysical Research Letters* **45**, 3001–8.
- Li XH, Li WX, Li ZX, Lo CH, Wang J, Ye MF and Yang YH** (2009) Amalgamation between the Yangtze and Cathaysia Blocks in South China: constraints from SHRIMP U–Pb zircon ages, geochemistry and Nd–Hf isotopes of the Shuangxiwu volcanic rocks. *Precambrian Research* **174**, 117–28.
- Li XH, Li ZX and Li WX** (2014) Detrital zircon U–Pb age and Hf isotope constrains on the generation and reworking of Precambrian continental crust in the Cathaysia Block, South China: a synthesis. *Gondwana Research* **25**, 1202–15.
- Li XH, Tang GQ, Gong B, Yang YH, Hou KJ, Hu ZC, Li QL, Liu Y and Li WX** (2013) Qinghu zircon: a working reference for microbeam analysis of U–Pb age and Hf and O isotopes. *Chinese Science Bulletin* **58**, 4647–54.
- Li ZX, Bogdanova SV, Collins AS, Davidson A, De Waele B, Ernst RE, Fitzsimons ICW, Fuck RA, Gladkochub DP, Jacobs J, Karlstrom KE, Lu S, Natapov LM, Pease V, Pisarevsky SA, Thrane K and Vernikovskiy V** (2008) Assembly, configuration and break-up history of Rodinia: a synthesis. *Precambrian Research* **160**, 179–210.
- Liu XM., Gao S, Diwu SR and Ling W** (2008) Precambrian crustal growth of Yangtze craton as revealed by detrital zircon studies. *American Journal of Science* **308**, 421–68.
- Ludwig KR** (2003) *User's Manual for Isoplot 3.00: A Geochronological Toolkit for Microsoft Excel*. Berkeley Geochronology Center, Special Publication no. 4.
- McDonough WF and Sun S** (1995) The composition of the Earth. *Chemical Geology* **120**, 223–53.
- McKerrow WS, Scotese CR and Brasier MD** (1992) Early Cambrian continental reconstructions. *Journal of the Geological Society, London* **149**, 599–606.
- Meinhold G, Bassis A, Hinderer M, Lewin A and Berndt J** (2021) Detrital zircon provenance of north Gondwana Palaeozoic sandstones from Saudi Arabia. *Geological Magazine* **158**, 442–58.
- Meinhold G, Hashemi Azizi SH and Berndt J** (2020) Permian–Triassic magmatism in response to Palaeotethys subduction and pre-Late Triassic arrival of northeast Gondwana-derived continental fragments at the southern Eurasian margin: detrital zircon evidence from Triassic sandstones of Central Iran. *Gondwana Research* **83**, 118–31.
- Meinhold G, Morton AC and Avigad D** (2013) New insights into peri-Gondwana paleogeography and the Gondwana super-fan system from detrital zircon U–Pb ages. *Gondwana Research* **23**, 661–5.

- Merdith AS, Williams SE, Collins AS, Tetley MG, Mulder JA, Blades ML, Young A, Armistead SE, Cannon J, Zahirovic S and Müller RD (2021) Extending full-plate tectonic models into deep time: linking the Neoproterozoic and the Phanerozoic. *Earth-Science Reviews* **214**, 103477. doi: [10.1016/j.earscirev.2020.103477](https://doi.org/10.1016/j.earscirev.2020.103477).
- Mergl M (2002) Linguliformean and craniiformean brachiopods of the Ordovician (Třenice to Dobrotiva formations) of the Barrandian, Bohemia. *Acta Museis Nationale Prague, Series B, Natural History* **58**, 1–82.
- Moghadam HS, Griffin W, Li XH, Santos JF, Karsli O, Stern RJ, Ghorbani G, Gain S, Murphy R and O'Reilly SY (2018) Crustal evolution of NW Iran: Cadomian arcs, Archean fragments and the Cenozoic magmatic flare-up. *Journal of Petrology* **58**, 2143–90.
- Moghadam HS, Li QL, Griffin WL, Karsli O, Santos JF, Ottley CJ, Ghorbani G, and O'Reilly SY (2020a) Tracking the birth and growth of Cimmeria: geochronology and origins of intrusive rocks from NW Iran. *Gondwana Research* **87**, 188–206.
- Moghadam HS, Li QL, Griffin WL, Stern RJ, Ishizuka O, Henry H, Lucci F, O'Reilly SY and Ghorbani G (2020b) Repeated magmatic buildup and deep “hot zones” in continental evolution: the Cadomian crust of Iran. *Earth and Planetary Science Letters* **531**, 115989. doi: [10.1016/j.epsl.2019.115989](https://doi.org/10.1016/j.epsl.2019.115989).
- Moghadam HS, Li XH, Griffin WL, Stern RJ, Thomsen TB, Meinhold G, Aharipour R and O'Reilly SY (2017) Early Paleozoic tectonic reconstruction of Iran: tales from detrital zircon geochronology. *Lithos* **268–271**, 87–101.
- Moghadam HS, Li XH, Ling XX, Stern RJ, Santos JF, Meinhold G, Ghorbani G and Shahabi S (2015) Petrogenesis and tectonic implications of Late Carboniferous A-type granites and gabbroanorthites in NW Iran: geochronological and geochemical constraints. *Lithos* **212–215**, 266–79.
- Mohajjel M, Fergusson C and Sahandi MR (2003) Cretaceous–Tertiary convergence and continental collision, Sanandaj–Sirjan Zone, western Iran. *Journal of Asian Earth Sciences* **21**, 397–412.
- Moosavi E, Mohajjel M and Rashidnejad-Omran N (2014) Systematic change in orientation of linear mylonitic fabrics: an example of strain partitioning during transpressional deformation in north Golpaygan, Sanandaj–Sirjan zone, Iran. *Journal of Asian Earth Sciences* **94**, 55–67.
- Morag N, Avigad D, Gerdes A, Belousova E and Harlavan Y (2011) Crustal evolution and recycling in the northern Arabian–Nubian Shield: new perspectives from zircon Lu–Hf and U–Pb systematics. *Precambrian Research* **186**, 101–16.
- Morag N, Avigad D, Gerdes A and Harlavand Y (2012) 1000–580 Ma crustal evolution in the northern Arabian–Nubian Shield revealed by U–Pb–Hf of detrital zircons from late Neoproterozoic sediments (Elat area, Israel). *Precambrian Research* **208–211**, 197–212.
- Moritz R, Ghazban F and Singer BS (2006) Eocene gold ore formation at Muteh, Sanandaj–Sirjan tectonic zone, eastern Iran: a result of late-stage extension and exhumation of metamorphic basement rocks within the Zagros orogen. *Economic Geology* **101**, 1497–524.
- Mouthereau F, Lacombe O and Vergés J (2012) Building the Zagros collisional orogen: timing, strain distribution and the dynamics of Arabia/Eurasia plate convergence. *Tectonophysics* **532–535**, 27–60.
- Müller KJ (1973) Late Cambrian and Early Ordovician conodonts from northern Iran. *Geological Survey of Iran, Report* **30**, 1–77.
- Murphy JB, Pisarevsky SA, Nance RD and Keppie JD (2004) Neoproterozoic–Early Paleozoic evolution of peri-Gondwanan terranes: implications for Laurentia–Gondwana connections. *International Journal of Earth Sciences* **93**, 659–82.
- Neubauer F (2014) Gondwana-land goes Europe. *Austrian Journal of Earth Sciences* **107**, 147–55.
- Nutman AP, Mohajjel M, Bennett VC and Fergusson CL (2014) Gondwanan Eoarchean–Neoproterozoic ancient crustal material in Iran and Turkey: zircon U–Pb–Hf isotopic evidence. *Canadian Journal of Earth Sciences* **51**, 272–85.
- Okada Y, Sawaki Y, Komiya T, Hirata T, Takahata N, Sano Y, Han J and Maruyama S (2014) New chronological constraints for Cryogenian to Cambrian rocks in the Three Gorges, Weng'an and Chengjiang areas, South China. *Gondwana Research* **25**, 1027–44.
- Paidar-Saravi H (1989) *Petrographisch-lagerstättenkundliche Untersuchungen an goldführenden Gesteinen im Muteh-Gebiet im Westen vom Zentraliran*. Heidelberg: Geowissenschaftliche Abhandlungen 33. Heidelberg: Ruprecht-Karls-Universität, 174 pp.
- Pallister JS, Stacey JS, Fischer LB and Premo WR (1988) Precambrian ophiolites of Arabia – geologic settings, U–Pb geochronology, Pb-isotope characteristics, and implications for continental accretion. *Precambrian Research* **38**, 1–54.
- Popov LE, Bassett MG, Holmer LE and Ghobadi Pour M (2009a) Early ontogeny and soft tissue preservation in siphonotretide brachiopods: new data from the Cambrian–Ordovician of Iran. *Gondwana Research* **16**, 151–61.
- Popov LE and Cocks LRM (2017) The World's second oldest strophomenoid-dominated benthic assemblage in the first Dapingian (Middle Ordovician) brachiopod fauna identified from Iran. *Journal of Asian Earth Sciences* **140**, 1–12.
- Popov LE, Ghobadi Pour M, Bassett MG and Kebria-ee M (2009b) Billingsellide and orthide brachiopods: new insights into earliest Ordovician evolution and biogeography from northern Iran. *Palaeontology* **52**, 35–52.
- Popov LE, Ghobadi Pour M and Hosseini M (2008) Early to Middle Ordovician lingulate brachiopods from the Lashkarak Formation, Eastern Alborz Mountains, Iran. *Alcheringa* **32**, 1–35.
- Popov LE, Hairapetian V, Ghobadi Pour M, Buttler C, Evans DH, Hejazi SH and Jahangir H (2014) Llandovery fauna of Iran during the post-extinction recovery. In *Abstract Volume and Proceedings of The Third International Symposium of the International Geosciences Programme Project 589 (IGCP-589). Development of the Asian Tethyan Realm: Genesis Process and Outcomes, Tehran, Iran, 19–26 October 2014*, pp. 105–10.
- Popov LE, Holmer LE, Bassett MG, Ghobadi Pour M and Percival IG (2013) Biogeography of Ordovician linguliform and craniiform brachiopods. In *Early Paleozoic Biogeography and Palaeogeography* (eds DAT Harper and T Servais), pp. 117–26. Geological Society of London, Memoirs no. 38.
- Popov LE, Holmer LE and Miller JF (2002) Lingulate brachiopods from the Cambrian–Ordovician boundary beds of Utah. *Journal of Paleontology* **76**, 211–28.
- Portner RA, Daczko NR, Murphy MJ and Pearson NJ (2011) Enriching mantle melts within a dying mid-ocean spreading ridge: insights from Hf-isotope and trace element patterns in detrital oceanic zircon. *Lithos* **126**, 355–68.
- Rachidnejad-Omran N, Emami MH, Sabzehei M, Rastad E, Bellon H and Pique A (2002) Lithostratigraphie et histoire paléozoïque à paléocène des complexes métamorphiques de la région de Muteh, zone de Sanandaj–Sirjan (Iran méridional). *Comptes Rendus Geoscience* **334**, 1185–91.
- Rahmati-Ilkhchi M, Faryad SW, Holub FV, Košler J and Frank W (2011) Magmatic and metamorphic evolution of the Shotur Kuh metamorphic complex (Central Iran). *International Journal of Earth Sciences* **100**, 45–62.
- Ramezani J and Tucker RD (2003) The Saghand Region, Central Iran: U–Pb geochronology, petrogenesis and implications for Gondwana Tectonics. *American Journal of Science* **303**, 622–65.
- Ranjan S, Upadhyay D, Pruseth KL and Nanda JK (2020) Detrital zircon evidence for change in geodynamic regime continental crust formation 3.7–3.6 billion years ago. *Earth and Planetary Science Letters* **538**, 116206. doi: [10.1016/j.epsl.2020.116206](https://doi.org/10.1016/j.epsl.2020.116206).
- Richards JP (2015) Tectonic, magmatic, and metallogenic evolution of the Tethyan orogeny: from subduction to collision. *Ore Geology Reviews* **70**, 323–45.
- Robinson FA, Foden JD, Collins AS and Payne JL (2014) Arabian Shield magmatic cycles and their relationship with Gondwana assembly: insights from zircon U–Pb and Hf isotopes. *Earth and Planetary Science Letters* **408**, 207–25.
- Rowland SM and Gangloff RA (1988) Structure and paleoecology of Lower Cambrian reefs. *Palaios* **3**, 111–35.
- Rowland SM and Shapiro RS (2002) Reef patterns and environmental influences in the Cambrian and Earliest Ordovician. In *Phanerozoic Reef Patterns* (eds W Kiessling, E Flügel and J Golonka), pp. 95–128. SEPM Special Publication no. 72.
- Rubatto D (2002) Zircon trace element geochemistry: partitioning with garnet and the link between U–Pb ages and metamorphism. *Journal of Chemical Geology* **184**, 123–38.

- Rubatto D and Hermann J** (2007) Experimental zircon/melt and zircon/garnet trace element partitioning and implications for the geochronology of crustal rocks. *Chemical Geology* **241**, 38–61.
- Saccani E, Azimzadeh Z, Dilek Y and Jahangiri A** (2013) Geochronology and petrology of the Early Carboniferous Misho Mafic Complex (NW Iran), and implications for the melt evolution of Paleo-Tethyan rifting in Western Cimmeria. *Lithos* **162**, 264–78.
- Şengör AMC** (1990) A new model for the late Paleozoic–Mesozoic tectonic evolution of Iran and implications for Oman. In *The Geology and Tectonics of the Oman Region* (eds AHF Robertson, MP Searle and AC Reis), pp. 797–831. Geological Society of London, Special Publication no. 49.
- Shabanian N, Davoudian AR, Azizi H, Asahara Y, Neubauer F, Genser J, Dong Y and Lee JKW** (2020) Petrogenesis of the Carboniferous Ghaleh-Dezh metagranite, Sanandaj–Sirjan zone, Iran: constraints from new zircon U–Pb and  $^{40}\text{Ar}/^{39}\text{Ar}$  ages and Sr–Nd isotopes. *Geological Magazine* **157**, 1823–52.
- Shahkarami S, Mángano MG and Buatois LA** (2017a) Discriminating ecological and evolutionary controls during the Ediacaran–Cambrian transition: trace fossils from the Soltanieh Formation of northern Iran. *Palaeogeography, Palaeoclimatology, Palaeoecology* **476**, 15–27.
- Shahkarami S, Mángano MG and Buatois LA** (2017b) Ichnostratigraphy of the Ediacaran–Cambrian boundary: new insights on lower Cambrian biozonations from the Soltanieh Formation of northern Iran. *Journal of Paleontology* **91**, 1178–98.
- Shakerardakani F, Li XH, Ling XX, Li J, Tang GQ, Liu Y and Monfaredi B** (2019) Evidence for Archean crust in Iran provided by ca. 2.7 Ga zircon xenocrysts within amphibolites from the Sanandaj–Sirjan zone, Zagros orogen. *Precambrian Research* **332**, 105390. doi: [10.1016/j.precamres.2019.105390](https://doi.org/10.1016/j.precamres.2019.105390).
- Shakerardakani F, Li XH, Neubauer F, Ling XX, Li J, Monfaredi B and Wu LG** (2020) Genesis of early Cretaceous leucogranites in the Central Sanandaj–Sirjan zone Iran: reworking of Neoproterozoic metasedimentary rocks in an active continental margin. *Lithos* **352–353**, 105330. doi: [10.1016/j.lithos.2019.105330](https://doi.org/10.1016/j.lithos.2019.105330).
- Shakerardakani F, Neubauer F, Bernroider M, Finger F, Hauzenberger CA, Genser J, Waitzinger M and Monfaredi B** (2021) Metamorphic stages in mountain belts during a Wilson cycle: A case study in the central Sanandaj–Sirjan zone (Zagros Mountains, Iran). *Geoscience Frontiers*. <https://doi.org/10.1016/j.gsf.2021.101272>.
- Shakerardakani F, Neubauer F, Bernroider M, von Quadt A, Peytcheva I, Liu X, Genser J, Monfaredi B and Masoudi F** (2017) Geochemical and isotopic evidence for Carboniferous rifting: mafic dykes in the central Sanandaj–Sirjan zone (Dorud–Azna, West Iran). *Geologica Carpathica* **68**, 229–47.
- Shakerardakani F, Neubauer F, Liu X, Bernroider M, Monfaredi B and von Quadt A** (2018) Tectonic significance of Triassic mafic rocks in the June Complex, Sanandaj–Sirjan zone, Iran. *Swiss Journal of Geosciences* **111**, 13–33.
- Shakerardakani F, Neubauer F, Masoudi F, Mehrabi B, Liu X, Dong Y, Mohajjel M, Monfaredi B and Friedl G** (2015) Panafrican basement and Mesozoic gabbro in the Zagros orogenic belt in the Dorud–Azna region (NW Iran): laser-ablation ICP–MS zircon ages and geochemistry. *Tectonophysics* **647–648**, 146–71.
- Sheikholeslami R, Bellon H, Emami H, Sabzehei M and Pique A** (2003) Nouvelles données structurales et datations  $^{40}\text{K}/^{40}\text{Ar}$  sur les roches métamorphiques de la région de Neyriz (zone de Sanandaj–Sirjan, Iran méridional). Leur intérêt dans le cadre du domaine néo-téthysien du Moyen-Orient. *Comptes Rendus Geoscience* **335**, 981–91.
- Shergold H, Cooper RA, MacKinnon DI and Yochelson EL** (1976) Late Cambrian Brachiopoda, Mollusca, and Trilobita from Northern Victoria Land, Antarctica. *Palaentology* **19**, 247–91.
- Shu L, Yao J, Wang B, Faure M, Charvet J and Chen Y** (2021) Neoproterozoic plate tectonic process and Phanerozoic geodynamic evolution of the South China Block. *Earth-Science Reviews* **216**, 103596. doi: [10.1016/j.earscirev.2021.103596](https://doi.org/10.1016/j.earscirev.2021.103596).
- Singh BP, Lokho K, Kishore N and Virmani N** (2014) Early Cambrian ichnofossils from the Mussoorie syncline and revision of trace-fossil biozonation of the Lesser Himalaya, India. *Acta Geologica Sinica* **88**, 380–93.
- Smith EF, Macdonald FA, Petach TA, Bold U and Schrag DP** (2015) Integrated stratigraphic, geochemical, and paleontological late Ediacaran to early Cambrian records from southwestern Mongolia. *Geological Society of America Bulletin* **128**, 442–68.
- Song SG, Niu YL, Wei CJ, Ji JQ and Su L** (2010) Metamorphism, anatexis, zircon ages and tectonic evolution of the Gongshan block in the northern Indochina continent—an eastern extension of the Lhasa Block. *Lithos* **120**, 327–46.
- Squire RJ, Campbell IH, Allen CM and Wilson CJL** (2006) Did the Transgondwanan Supermountain trigger the explosive radiation of animals on earth? *Earth and Planetary Science Letters* **250**, 116–33.
- Stampfli GM, Hochard C, Vérard C, Wilhem C and von Raumer J** (2013) The formation of Pangea. *Tectonophysics* **593**, 1–19.
- Steiner M, Li G, Qian Y, Zhu M and Erdtmann BD** (2007) Neoproterozoic to early Cambrian small shelly fossil assemblages and a revised biostratigraphic correlation of the Yangtze Platform (China). *Palaeogeography, Palaeoclimatology, Palaeoecology* **254**, 67–99.
- Stephan T, Kroner U and Romer RL** (2019) The pre-orogenic detrital zircon record of the Peri-Gondwanan crust. *Geological Magazine* **156**, 281–307.
- Stern RJ** (1994) Arc assembly and continental collision in the Neoproterozoic East African Orogen: implications for the assembly of Gondwanaland. *Annual Review of Earth and Planetary Sciences* **22**, 319–51.
- Stevens Goddard AL, Trop JM and Ridgway KD** (2018) Detrital zircon record of a Mesozoic collisional forearc basin in south central Alaska: the tectonic transition from an oceanic to continental arc. *Tectonics* **37**, 529–57.
- Stöcklin J** (1968) Structural history and tectonics of Iran: a review. *American Association of Petroleum Geologists Bulletin* **52**, 1229–58.
- Thiele O** (1966) Zum Alter der Metamorphose in Zentraliran. *Mitteilungen der geologischen esellschaft (Wien)* **58**, 87–101.
- Torsvik TH** (1998) Palaeozoic palaeogeography: a north Atlantic viewpoint. *GFF* **120**, 109–18.
- Torsvik TH and Cocks LRM** (2013) Gondwana from top to base in space and time. *Gondwana Research* **24**, 999–1030.
- von Raumer JF, Bussy F, Schaltegger U, Schulz B and Stampfli GM** (2013) Pre-Mesozoic Alpine basements—their place in the European Paleozoic framework. *Geological Society of America Bulletin* **125**, 89–108.
- Wang GG, Ni P, Zhu AD, Wang XL, Li L, Hu JS, Lin WH and Huang B** (2018) 1.01–0.98 Ga mafic intra-plate magmatism and related Cu–Au mineralization in the eastern Jiangnan orogen: evidence from Liujia and Tieshajie basalts. *Precambrian Research* **309**, 6–21.
- Wang MX, Wang CY and Zhao JH** (2013) Zircon U/Pb dating and Hf–O isotopes of the Zhouan ultramafic intrusion in the northern margin of the Yangtze Block, SW China: constraints on the nature of mantle source and timing of the supercontinent Rodinia breakup. *Chinese Science Bulletin* **58**, 777–87.
- Wang W, Zhou M, Chu Z, Xu J, Li C, Luo T and Guo J** (2020) Constraints on the Ediacaran–Cambrian boundary in deep-water realm in South China: evidence from zircon CA–ID–TIMS U–Pb ages from the topmost Liuchapo Formation. *Science China Earth Sciences* **63**, 1176–87.
- Wang YJ, Zhang F, Fan W, Zhang G, Chen S, Cawood PA and Zhang A** (2010) Tectonic setting of the South China Block in the early Paleozoic: resolving intracontinental and ocean closure models from detrital zircon U–Pb geochronology. *Tectonics* **29**, TC6020. doi: [10.1029/2010TC002750](https://doi.org/10.1029/2010TC002750).
- Wang YJ, Zhu WG, Huang HQ, Zhong H, Bai ZJ, Fan HP and Yang YJ** (2019) Ca. 1.04 Ga hot Grenville granites in the western Yangtze Block, southwest China. *Precambrian Research* **328**, 217–34.
- Weber B, Steiner M, Evseev S and Yergaliev G** (2013) First report of a Meishucun-type early Cambrian (Stage 2) ichnofauna from the Malý Karatau area (SE Kazakhstan): palaeoichnological, palaeoecological and palaeogeographical implications. *Palaeogeography, Palaeoclimatology, Palaeoecology* **392**, 209–31.
- Wendt J, Kaufmann B, Belka Z, Farsan N and Karimi Bavandpur A** (2002) Devonian/Lower Carboniferous stratigraphy, facies patterns and palaeogeography of Iran. Part I. Southeastern Iran. *Acta Geologica Polonica* **52**, 129–68.
- Wendt J, Kaufmann B, Belka Z, Farsan N and Karimi Bavandpur A** (2005) Devonian/Lower Carboniferous stratigraphy, facies patterns and palaeogeography of Iran. Part II. Northern and central Iran. *Acta Geologica Polonica* **55**, 31–97.

- Wiedenbeck M, Allé P, Corfu F, Griffen WL, Meier M, Oberli F, von Quadt A, Roddick JC and Spiegel W (1995) Three natural zircon standards for U–Th–Pb, Lu–Hf, trace element, and REE analyses. *Geostandards and Geoanalytical Research* **19**, 1–23.
- Yang C, Li XH, Li ZX, Zhu M and Lu K (2020) Provenance evolution of age-calibrated strata reveals when and how South China Block collided with Gondwana. *Geophysical Research Letters* **47**, e2020GL090282. doi: [10.1029/2020GL090282](https://doi.org/10.1029/2020GL090282).
- Yang C, Zhu M, Condon DJ and Li XH (2017) Geochronological constraints on stratigraphic correlation and oceanic oxygenation in Ediacaran–Cambrian transition in South China. *Journal of Asian Earth Sciences* **140**, 75–81.
- Yang YN, Wang XC, Li QL and Li XH (2016) Integrated in situ U–Pb age and Hf–O analyses of zircon from Suixian Group in northern Yangtze: new insights into the Neoproterozoic low- $\delta^{18}\text{O}$  magmas in the South China Block. *Precambrian Research* **273**, 151–64.
- Yao WH, Li ZX, Li WX, Li XH and Yang JH (2014) From Rodinia to Gondwanaland: a tale of detrital zircon provenance analyses from the southern Nanhua basin, South China. *American Journal of Science* **314**, 278–313.
- Yeshanew FG, Pease V, Whitehouse MJ and Al-Khribash S (2015) Zircon U–Pb geochronology and Nd isotope systematics of the Abas terrane, Yemen: implications for Neoproterozoic crust reworking events. *Precambrian Research* **267**, 106–20.
- Yu JH, O'Reilly SY, Wang L, Griffen WL, Zhang M, Wang R, Jiang S and Shu L (2008) Where was South China in the Rodinia supercontinent? Evidence from U–Pb geochronology and Hf isotopes of detrital zircons. *Precambrian Research* **164**, 1–15.
- Yuan HL, Gao S, Liu XM, Li HM, Günther D and Wu FY (2004) Accurate U–Pb age and trace element determinations of zircon by laser ablation–inductively coupled plasma mass spectrometry. *Geostandards and Geoanalytical Research* **28**, 353–70.
- Žák J, Svojtka M, Gerdjikov I, Kounov A and Vangelov DA (2021) The Balkan terranes: a missing link between the eastern and western segments of the Avalonian–Cadomian orogenic belt? *International Geology Review*, published online 12 January 2021. doi: [10.1080/00206814.2020.1861486](https://doi.org/10.1080/00206814.2020.1861486).
- Zanchetta S, Berra F, Zanchi A, Bergomi M, Caridroit M, Nicora A and Heidarzadeh G (2013) The record of the Late Palaeozoic active margin of the Palaeotethys in NE Iran: constraints on the Cimmerian orogeny. *Gondwana Research* **24**, 1237–66.
- Zanchetta S, Zanchi A, Villa IM, Poli S and Muttoni G (2009) The Shanderman eclogites: a Late Carboniferous high-pressure event in the NW Talesh Mountains (NW Iran). In *South Caspian to Central Iran Basins* (eds M-F Brunet, M Wilmsen and JW Granath), pp. 57–78. Geological Society of London, Special Publication no. 312.
- Zanchi A, Zanchetta S, Berra F, Mattei M, Garzanti E, Molyneux S, Nawab A and Sabouri J (2009a) The Eo-Cimmerian (Late? Triassic) orogeny in North Iran. In *South Caspian to Central Iran Basins* (eds M-F Brunet, M Wilmsen and JW Granath), pp. 31–55. Geological Society of London, Special Publication no. 312.
- Zanchi A, Zanchetta S, Garzanti E, Balini M, Berra F, Mattei M and Muttoni G (2009b) The Cimmerian evolution of the Nakhlak–Anarak area, central Iran, and its bearing for the reconstruction of the history of the Eurasian margin. In *South Caspian to Central Iran Basins* (eds M-F Brunet, M Wilmsen and JW Granath), pp. 261–86. Geological Society of London, Special Publication no. 312.
- Zhan R and Jin J (2014) Early–Middle Ordovician brachiopod dispersal patterns in South China. *Integrative Zoology* **9**, 121–40.
- Zhang J (1995) Ordovician phosphatic inarticulate brachiopods from Cili, Hunan. *Acta Palaeontologica Sinica* **34**, 152–70 (in Chinese with English summary).
- Zhang SH (2004) South China's Gondwana connection in the Paleozoic: paleomagnetic evidence. *Progress in Natural Science* **14**, 85–90.
- Zhang Z, Xiao W, Majidifard MR, Zhu R, Wan B, Ao S, Chen L, Rezaeian M and Esmaili R (2017) Detrital zircon provenance analysis in the Zagros Orogen, SW Iran: implications for the amalgamation history of the Neo-Tethys. *International Journal of Earth Sciences* **106**, 1223–38.
- Zhao JH, Zhou MF, Zheng JP and Griffen WL (2013) Neoproterozoic tonalite and Trondhjemite in the Huangling complex, South China: crustal growth and reworking in a continental arc environment. *American Journal of Science* **313**, 540–83.
- Zhu M (1997) Precambrian–Cambrian trace fossils from eastern Yunnan, China: implications for Cambrian explosion. *Bulletin of National Museum of Natural Science* **10**, 275–312.
- Zoleikhaei Y, Mulder JA and Cawood PA (2020) Integrated detrital rutile and zircon provenance reveals multiple sources for Cambrian sandstones in North Gondwana. *Earth-Science Reviews* **213**, 103462. doi: [10.1016/j.earscirev.2020.103462](https://doi.org/10.1016/j.earscirev.2020.103462).

### Appendix 1.: Laser ablation ICP-MS U–Pb analytical techniques, Northwest University, Xi'an

Zircons were separated from the one sample from the Dorud area (LJ-140) in the laboratory of the Geography and Geology Department of Salzburg University, Austria. The selected zircon grains were dated *in situ* on an excimer (193 nm wavelength) laser ablation inductively coupled plasma mass spectrometer (LA-ICP-MS) at the State Key Laboratory of Continental Dynamics, Northwest University. The ICP-MS used is an Agilent 7500a (with shield torch). The unique shield torch increases analytical sensitivity by a factor of >10 (for example, 4500 cps/ppm  $^{238}\text{U}$  at a spot size of 40  $\mu\text{m}$  and laser frequency of 10 Hz), which is important for LA-ICP-MS. The GeoLas 200M laser ablation system (MicroLas, Göttingen, Germany) was used for the laser ablation experiments. Helium was used as the carrier gas. The used spot size and laser frequency were set at 40  $\mu\text{m}$  and 10 Hz, respectively. The data acquisition mode was peak jumping (20 ms per isotope each cycle). Raw count rates were measured for  $^{29}\text{Si}$ ,  $^{204}\text{Pb}$ ,  $^{206}\text{Pb}$ ,  $^{207}\text{Pb}$ ,  $^{208}\text{Pb}$ ,  $^{232}\text{Th}$  and  $^{238}\text{U}$ . U, Th and Pb concentrations were calibrated by using  $^{29}\text{Si}$  as an internal standard and NIST SRM 610 as the reference standard. Each analysis consisted of 30 s gas blank and 40 s signal acquisition. High-purity argon was used together with a custom helium filtration column, which resulted in  $^{204}\text{Pb}$  and  $^{202}\text{Hg}$  being less than 100 cps in the gas blank. Therefore, the contribution of  $^{204}\text{Hg}$  to  $^{204}\text{Pb}$  as revealed by detrital zircon studies was negligible and no correction was made.  $^{207}\text{Pb}/^{206}\text{Pb}$ ,  $^{206}\text{Pb}/^{238}\text{U}$ ,  $^{207}\text{Pb}/^{235}\text{U}$  and  $^{208}\text{Pb}/^{232}\text{Th}$  ratios, calculated using GLITTER 4.0 (Macquarie University), were corrected for both instrumental mass bias and depth-dependent elemental and isotopic fractionation using Harvard zircon 91500 as an external standard. The ages were calculated using Isoplot 3 (Ludwig, 2003). Our measurement of TEMORA 1 as an unknown yielded a weighted  $^{206}\text{Pb}$ – $^{238}\text{U}$  age of  $415 \pm 4$  Ma (MSWD = 0.112,  $n = 24$ ) (Yuan *et al.* 2004), which is in good agreement with the recommended ID-TIMS age of  $416.75 \pm 0.24$  Ma (Black *et al.* 2003). Analytical details for age and trace and rare earth element determinations of zircons are reported in Yuan *et al.* (2004). Common Pb corrections were made following the method of Andersen (2002). Because measured  $^{204}\text{Pb}$  usually accounts for <0.3 % of the total Pb, the correction is insignificant in most cases.

### Appendix 2.: Laser ablation ICP-MS U–Pb analytical techniques, China University of Geosciences, Beijing

The separated detrital zircons from two garnet–micaschist samples were embedded in epoxy resin discs and polished down to about half-sections to expose the grain interiors, and then imaged under reflected and transmitted light and by using CL. U(–Th)–Pb analyses of the detrital zircons were carried out on an Agilent-7500a quadrupole inductively coupled plasma mass spectrometry (LA-

ICP-MS) coupled with a New Wave SS UP193 laser sampler at the Elemental Geochemistry Lab of the Institute of Earth Sciences, China University of Geosciences, Beijing. For the present work, the laser spot size was set to  $\sim 36\ \mu\text{m}$  for one sample (GQ-21) and to  $25\ \mu\text{m}$  for sample GQ-12 with a small size of zircons; the laser energy density was set at  $8.5\ \text{J cm}^{-2}$  and repetition rate at 10 Hz. The procedure of laser sampling includes 5-s pre-ablation, 20-s sample-chamber flushing and 40-s sampling ablation. The ablated material is carried into the ICP-MS by the high-purity helium gas stream with a flux of  $0.8\ \text{L min}^{-1}$ . The whole laser path was fluxed with  $\text{N}_2$  ( $15\ \text{L min}^{-1}$ ) and Ar ( $1.15\ \text{L min}^{-1}$ ) in order to increase energy stability. The counting time for U, Th,  $^{204}\text{Pb}$ ,  $^{206}\text{Pb}$ ,

$^{207}\text{Pb}$  and  $^{208}\text{Pb}$  is 20 ms, and is 15 ms for other elements. Calibrations for the zircon analyses were carried out using NIST 610 glass as an external standard and Si as an internal standard. U–Pb isotope fractionation effects were corrected using zircon 91500 (Wiedenbeck *et al.* 1995) as an external standard. The zircon TEMORA (417 Ma, Black *et al.* 2003) and Qinghu ( $159.5 \pm 0.2\ \text{Ma}$ ; Li *et al.* 2013) were used as the secondary standards to supervise the deviation of age measurement/calculation. Data reduction was carried out on the software GLITTER (version 4.4, Macquarie University). The common lead correction was made following Andersen (2002), and Isoplot 3 (Ludwig, 2003) was used for age calculations and plots of concordia diagrams.